

The Role of Vasculature During the Development of Intramembranous Bones of the
Chick, *Gallus gallus*

by

James Patrick Jabalee

Submitted in partial fulfillment of the requirements for the degree of Master of Science

at

Dalhousie University

Halifax, Nova Scotia

July 2014

I dedicate this thesis to the memory of Ellen and Roderick Hood.

Table of contents

List of Tables.....	vi
List of Figures.....	vii
Abstract.....	viii
List of Abbreviations Used.....	ix
Acknowledgements.....	xi
Chapter 1.0: Introduction.....	1
1.1 The Vertebrate Skeleton.....	2
1.2 Mesenchymal Condensations.....	4
1.3 Chick Scleral Ossicles.....	6
1.4 The Role of Vasculature in Bone Development.....	12
1.5 Hypotheses and Objectives.....	20
Chapter 2.0: Materials and Methods.....	22
2.1 Chicken Embryos.....	22
2.2 Blood Vessel Visualization using Spotlitter Highlighter Ink.....	22
2.2.1 Preparation of Microcapillary Pipettes.....	22
2.2.2 Preparation of Ink.....	23
2.2.3 Ink Injection.....	23
2.3 Probe Preparation, Whole Mount <i>In Situ</i> Hybridization and Cryosectioning.....	24
2.3.1 Molecular Cloning.....	24
2.3.2 Isolation of Plasmid DNA.....	25

2.3.3	Linearization of <i>vegfa</i> cDNA.....	26
2.3.4	Purification Of Linearized <i>vegfa</i> cDNA.....	27
2.3.5	Gel Electrophoresis.....	27
2.3.6	Probe Synthesis.....	27
2.3.7	Whole Mount <i>In Situ</i> Hybridization.....	29
2.3.8	Cryosectioning of <i>In Situ</i> -Stained Embryos.....	31
2.4	Vegf Inhibitor Application.....	31
2.4.1	Preparation of Vegf Inhibitor.....	31
2.4.2	Preparation of Beads for Implantation.....	32
2.4.3	Preparation of Tungsten Needles.....	33
2.4.4	Membrane Dissection.....	33
2.4.5	Bead Implantation.....	34
2.4.6	Statistical Analysis.....	34
2.4.7	Alkaline Phosphatase Staining.....	35
Chapter 3.0:	Results.....	36
3.1	Mapping the Growth of Scleral Vasculature.....	36
3.2	<i>vegfa In Situ</i> Hybridization.....	39
3.2.1	HH 35 – Induction.....	39
3.2.2	HH 36.5 – Condensation.....	40
3.2.3	HH 37 – Osteoid Deposition.....	44
3.2.4	HH 38.5 – Mineralization.....	44
3.2.5	Summary of <i>In Situ</i> Results.....	48
3.3	Bead Implantation.....	48

3.3.1	Effect of Sflt-1 on Scleral Vasculature.....	48
3.3.2	Effect of Sflt-1 on Scleral Ossicle Development.....	53
Chapter 4.0:	Discussion.....	65
4.1	Conjunctival Papillae and Surrounding Tissues Regulate Growth of Scleral Vasculature.....	65
4.2	Expansion of Avascular Zones is Not Sufficient to Promote Osteogenesis....	70
4.3	Vegf Regulates the Early Stages of Intramembranous Ossification <i>In Vivo</i> ...	73
4.4	Implantation of sFlt-1-Soaked Beads Results in Widespread, Rather Than Local, Effects.....	76
4.5	Conclusions.....	79
References.....		83
Appendix A –	Preparing LB Broth and Agar Plates.....	93
Appendix B -	Cloning.....	94
Appendix C –	Digestion and Clean-Up of Plasmid DNA.....	97
Appendix D –	Probe Preparation.....	98
Appendix E –	Dot Blot.....	99
Appendix F –	Whole Mount <i>In Situ</i> Hybridization.....	103
Appendix G –	Protocol for (3-Aminopropyl)Triethoxysilane (APTES)-Coated Slides..	111
Appendix H –	sFlt-1 Implantation Raw Data and Statistical Analysis.....	112
Appendix I –	Severity of Ossicle Mispatterning.....	116

List of Tables

Table 1	Measurement of the area of the avascular zone surrounding the papilla of the bead implanted (right) eye divided by the area of the equivalent papilla of the contralateral (left) eye at 1 day post-surgery.....	50
Table 2	Common ossicle mispatterning.....	55
Table 3	Relative frequency of the severity of ossicle mispatterning in sFlt-1 versus 1x PBS implanted and contralateral unimplanted eyes at 1 day post-surgery.....	59
Table 4	Relative frequency of the severity of ossicle mispatterning in sFlt-1 versus 1x PBS implanted and contralateral unimplanted eyes at 2 days post-surgery.....	61
Table 5	Average severity of ossicle mispatterning in sFlt-1 and 1x PBS implanted embryos at 1-2 days post-surgery.....	64
Table 6	Summary of developmental events during the formation of scleral ossicles.....	81

List of Figures

Figure 1	Summary of scleral ossicle development from HH 35-38.5 (day 9 – 12.5).....	11
Figure 2	Vegf signaling.....	17
Figure 3	Vascular growth in the sclera of the chick eye.....	38
Figure 4	<i>Vegfa in situ</i> hybridization, HH 35.....	41
Figure 5	<i>Vegfa in situ</i> hybridization, HH 36.5.....	43
Figure 6	<i>Vegfa in situ</i> hybridization, HH 37.....	46
Figure 7	<i>Vegfa in situ</i> hybridization, HH 38.5.....	47
Figure 8	Effect of sFlt-1-soaked bead implantation on scleral vasculature.....	52
Figure 9	Classifications of ossicle severity, HH 36.5 – 37.....	58
Figure 10	Severity of ossicle mispatterning in sFlt-1 versus 1x PBS implanted embryos at 1 day post-surgery.....	60
Figure 11	Severity of ossicle mispatterning in sFlt-1 versus 1x PBS implanted embryos at 2 days post-surgery.....	62

Abstract

Intramembranous bone development is a complex multi-step process which relies on extensive interactions between bone cells and surrounding tissue types. The embryonic vasculature, composed primarily of vascular endothelial cells, is well known to play a key role in regulating bone development via endochondral ossification; however, its role during intramembranous ossification remains poorly understood, and *in vivo* studies are lacking. Here I use the scleral ossicles of the domestic chick (*Gallus gallus*), a ring of intramembranous bones located in the sclera of the eye, to investigate the role of vasculature in intramembranous bone development *in vivo*. My results indicate that vasculature begins to fill the posterior sclera at HH 35 and forms distinct avascular zones around the conjunctival papillae, structures involved in the induction of the scleral ossicles. Posteriorly, these avascular zones are obliterated by HH 36.5, concomitant with the end of ossicle induction. *In situ* hybridization and bead implantation experiments suggest a key role for vascular endothelial growth factor (Vegf) in coordinating vascular and scleral ossicle development. *Vegfa* is expressed in the conjunctival papillae and the surrounding mesenchyme during ossicle induction and vascular growth, and is downregulated thereafter. Localized knockdown of Vegf signaling via bead implantation results in both an expansion of the avascular zone and mispatterning of the scleral ossicles, suggesting a key role for Vegf in regulating vascular growth and ossicle development. This work provides important insights into the complex relationship between bone and vasculature during development of chick scleral ossicles and intramembranous bones in general.

List of Abbreviations Used

AP – alkaline phosphatase

APTES – (3-aminopropyl)triethoxysilane

BCIP – 5-bromo-4-chloro-3-indoyl phosphate

Bmp-2 – bone morphogenetic protein 2

BSA – bovine serum albumin

CAM – chorioallantoic membrane

Cy3 – cyanine 3

DEPC – diethyl pyrocarbonate

dH₂O – distilled water

DIG – digoxigenin

Dps – days post-surgery

E. coli – *Escherichia coli*

EDTA – ethylenediaminetetraacetic acid

EtOH – ethanol

FITC – fluorescein isothiocyanate

GFP – green fluorescent protein

HH – Hamburger and Hamilton

Hif – hypoxia inducible factor

HSPG – heparan sulphate proteoglycan

Ihh – indian hedgehog

LB – Luria Bertani

MeOH – methanol

NBF – neutral buffered formalin

NBT – nitro blue tetrazolium

Nrp1 – neuropilin 1

PBS – phosphate buffered saline

PBST – phosphate buffered saline with TWEEN 20

PFA – paraformaldehyde

Ptc-1 – patched-1

PVA – polyvinyl alcohol

RNase – ribonuclease

RPE – retinal pigmented epithelium

Runx2 – runt-related transcription factor 2

SDS – sodium dodecyl sulfate

sFlt-1 – soluble fms-like tyrosine kinase-1

Shh – sonic hedgehog

TBST – tris buffered saline with TWEEN 20

vegfa – vascular endothelial growth factor A (gene)

Vegf – vascular endothelial growth factor (protein)

Vegfr – vascular endothelial growth factor receptor

Acknowledgements

First and foremost I would like to thank my supervisor, Tamara Franz-Odenaal. It is thanks to your guidance and support that this project was possible. Dedication, critical thinking and attention to detail are just a few of the many things I've learned from you over the years that I will take with me into the future. The experiences I've had and the goals I've achieved during my time in your lab are what allow me to call myself a scientist.

To my committee, Boris Kablar, Kazue Semba and Sophia Stone, thank you for your words of encouragement and insight which have helped to shape this project. Kazue, thank you for helping me to get settled at Dal, helping me tackle the administrative side of student life, and for joining my committee when I needed it most. Boris and Sophia, thank you for allowing me to learn from you both inside the classroom and out, and for inspiring me with your passion for science. I would also like to thank Dr. Todd Camenisch and Derrick Broka (University of Arizona) for providing me with *vegfa* plasmid and Dr. Ilya Blum (Mount Saint Vincent University) for advice regarding statistical analysis.

To the people with whom I spend most of my time – my labmates – thank you! You have all had a positive impact on this project and my life in general. Karyn, whether in regard to writing, literature or experimental technique you always have the answers to my questions. Your help, guidance and positivity have been invaluable. Sew, you have been a source of constant wisdom. There is no problem that can't be solved by chatting with you! Megan and Kellie, ever since my first day in the lab you have been both role models and friends. Thank you to Bev, Christine, Jade, Kaity, Greg and Matt for your support and for making the lab a truly fun place to work.

Finally, thank you to my family. Mom and Dad, you have provided me with everything I could ever need or want. Because of you I am able to follow my dreams. Kaela, thank you for putting up with my workaholism. You have not only made this possible, but worthwhile as well. Only another decade or so of school to go, I promise!

Chapter 1.0: Introduction

Bone development is regulated by precise spatiotemporal interactions between skeletal cells and surrounding cell and tissue types, including epithelia (Pinto and Hall, 1991; MacDonald and Hall, 2001), skeletal muscle (Hall and Herring, 1990; Rot-Nikcevic et al. 2006), nervous tissue (Garol et al., 1978), and vascular endothelial cells (Yin and Pacifici, 2001; Ramasamy et al., 2014). In the absence of these interactions, bones develop abnormally, or, in some cases, not at all.

Vascular endothelial cells have received increased attention in recent years due to a surge of evidence revealing their importance in regulating the activities of bone and cartilage cells (Riddle et al., 2010; Araldi and Schipani, 2010; Percival and Richtsmeier, 2013). These data suggest that blood vessels not only provide metabolic support to developing and adult bone tissues, but also provide skeletal cells with chemical cues which influence their survival (Schipani et al., 2001; Zelzer et al., 2004; Street and Lenehan, 2009), proliferation (Schipani et al., 2001; von Schroeder et al., 2003), differentiation (Midy and Plouët, 1994; Deckers et al., 2000; Liu et al., 2012) and synthetic activities (Myllyharju and Schipani, 2010; Bentovim and Zelzer, 2012). Blood vessels are required for the replacement of cartilage by bone (a process called endochondral ossification) as they deliver both cartilage-degrading chondroclasts and bone-forming osteoblasts to the primary ossification center (Maes et al, 2010). In addition to their role in the formation of embryonic bone, endothelial cells play key roles during fracture repair (Maes et al., 2010) and distraction osteogenesis (Pacicca et al., 2003; Byun et al., 2006; Jacobsen et al., 2008), a surgical procedure which involves slowly separating the fractured ends of a bone, in adults.

Thus far, the majority of research regarding vascular-skeletal interactions have focused on the elements of the limb, which first form a cartilaginous template before replacement by bone during the process of endochondral ossification. In contrast, the flat bones of the skull (calvariae), which form directly (without a cartilaginous precursor) via the process of intramembranous ossification, have received comparatively very little attention. The purpose of the research described herein is to provide insight into the relationship between vasculature and intramembranous bones, with a specific focus on the early phases of bone development, including patterning, formation of mesenchymal condensations, and osteoblast differentiation. Unlike many previous studies, which make use of various cell and tissue culture systems, this work was performed *in vivo* using chick scleral ossicles as a model. This will allow for a better understanding of the relationship between vasculature and bone during normal embryonic development, without the complications introduced by *in vitro* strategies.

1.1 The Vertebrate Skeleton

Bones can be described according to a number of developmental features, including germ layer origin (mesoderm or neural crest), shape (flat, long, short, irregular), position in the body (axial or appendicular) and mode of development (intramembranous or endochondral). The two most studied areas of the skeleton are the calvariae and the limb, described in turn below.

The calvariae are a set of flat bones which serve to support and protect the delicate soft tissues of the head, including the brain and sense organs. Unlike the bones of the limb, which are derived entirely from mesoderm, the calvariae are derived from both

mesoderm and neural crest (Noden and Trainor, 2005; Evans and Noden, 2006). The neural crest consists of a migratory population of pluripotent cells which break away from the edges of the neural tube during neurulation (reviewed in Takahashi et al., 2013). Driven by chemoattractive and chemorepulsive cues produced by other tissues, neural crest cells migrate throughout the body and give rise to a plethora of structures, including connective tissues of the head (Theveneau and Mayor, 2012; Takahashi et al., 2013). In the mouse, the frontal bone is derived entirely from the neural crest, whereas the parietal bone is derived entirely from mesoderm (Jiang et al., 2002). The situation is different in the chick, in which the anterior portion of the frontal bone is derived from neural crest whereas the posterior portion of the same bone is derived from mesoderm (Evans and Noden, 2006). The focus of this thesis is specifically on cranial neural crest-derived intramembranous bones, a category which includes chick scleral ossicles (described below). Despite their germ layer of origin, all calvarial bones ossify directly within a connective tissue membrane, a process termed intramembranous ossification.

Compared to the bones of the skull, the long bones of the limb receive significantly more attention in the literature. As such, it is useful to have a basic understanding of this system, since much of the background regarding bone development comes from studies of the limb skeleton. Most of the bones of the limb (excluding those of the wrist) are long bones, which consist of a shaft-like diaphysis bordered on each end by a knob-like epiphysis. As mentioned, the bones of the limb are derived from mesoderm, with no contribution from the neural crest. The elements of the limb are initially formed from cartilage, and it is during chondrogenesis that many of the key events in development occur, such as patterning and morphogenesis. Endochondral

ossification is initiated by enlarged chondrocytes located in the center of the element termed the hypertrophic zone. In response to factors secreted by hypertrophic chondrocytes, the hypertrophic zone is invaded by vasculature carrying cartilage-degrading chondroclasts, which degrade the cartilage template, and osteoprogenitors, which differentiate into osteoblasts and lay down bone tissue (Maes et al., 2010). Bones formed in this manner retain the basic shape of the cartilage template which they replaced.

1.2 Mesenchymal Condensations

The first step in the development of skeletal tissue (bone and cartilage) is the formation of mesenchymal condensations (reviewed in Hall and Miyake, 1992, 1995, 2000; Franz-Odenaal, 2011a). Condensations, which consist of areas of tightly packed, undifferentiated mesenchymal cells, form the raw material from which the skeleton is built. It is during this phase that many key features of the element, including shape, size and location, are largely determined. Numerous skeletal disorders can be traced back to cellular changes which occur during condensation, serving to underscore the importance of this phase of skeletal development (Grüneberg, 1963). For instance, *taplid*³ mutant chicks exhibit severe alterations of the limb skeleton, including polydactyly, fusion of the radius and ulna, and fusion of the carpals and metacarpals (Hall and Miyake, 1992). This phenotype has been linked to alterations in the level of a key cell adhesion molecule, neural cell adhesion molecule (NCAM), normally expressed by the cells of a condensation (Hall and Miyake, 2000). Altered levels of NCAM result in an abnormal allocation of cells into condensations, ultimately giving rise to altered skeletal elements

(Ede and Kelly, 1964). Condensations also have evolutionary importance (Hall, 1975). Reducing cell number below a particular threshold has been shown to result in absence of the skeletal element, as occurs in the Phocomelia mutant mouse (Fitch, 1957), and this has been proposed as a mechanism for loss of elements over evolution (Atchley and Hall, 1991). Additionally, fusion or splitting of condensations, which occurs during normal development of many bones, has been proposed as another mechanism by which skeletal elements may be gained or lost (Franz-Odenaal, 2011a). Finally, changes in the expression of key patterning genes, such as Hox genes, can result in duplications of skeletal elements or homeotic transformation of one element into another (e.g., Gendron-Maguire et al., 1994; Rijli et al., 1994).

Mesenchymal cells are instructed to condense via an epithelial-mesenchymal interaction. In response to this epithelial signal, cells may migrate towards a center, fail to migrate away from a center, and/or undergo proliferation to ultimately give rise to a condensation (Hall and Miyake, 1995, 2000). During chondrogenesis, it is well established that prechondrocyte differentiation follows, and is triggered by, condensation (Hall and Miyake, 2000). The situation is reversed during osteogenesis: alkaline phosphatase-positive preosteoblasts of the chick mandible can be seen prior to condensation (but after epithelial-mesenchymal interaction; Dunlop and Hall, 1995). This epithelial-mesenchymal interaction serves to regulate both the position and the timing of condensation initiation.

Condensation plays a key role in regulating the size of the resulting skeletal element. Condensation brings cells of similar differentiation potential into close contact with one another, allowing differentiation to occur simultaneously (Coelho and Kosher,

1991; Hall and Miyake, 1992). In order for differentiation to occur, a critical cell number must be reached, and experimentally increasing or decreasing condensation size results in an abnormally sized element (Grüneberg, 1963). Size changes can be achieved by altering the level of a number of different types of molecules, including cell adhesion molecules, such as NCAM; cell signalling molecules, such as Bmp-2 and 4; and extracellular matrix molecules, such as fibronectin (see Hall and Miyake, 2000 for specific examples). Although remodeling may alter the shape of a bone throughout life, condensations are thought to approximate the basic shape of the skeletal element to which they will give rise (Hall, 1975). For instance, one can clearly discern the shape and position of each of the digits of the hand in tissue section before any skeletal tissue is formed by recognizing areas of high cell density (condensations).

1.3 Chick Scleral Ossicles

The chick embryo has been an important model in the study of developmental biology for hundreds of years (Stern, 2005). In addition to being easily obtained in large quantities, a key advantage of the chick embryo is that it develops inside of an egg, rather than the mother's womb. Partial or complete removal of the egg shell can be performed without disrupting development, thereby making the embryo easily accessible for both observation and physical manipulation.

The sclerotic ring, formed from overlapping plates of bone (ossicles) located in the sclera of the eye, was first described in depth by P.D.F Murray in the early 1940's (Murray, 1941, 1943). Like the calvariae, scleral ossicles are flat, intramembranous bones derived from the neural crest (Franz-Odenaal, 2011b). As such, they are a useful model

to further our understanding of the development of the skull. Additionally, scleral ossicles are interesting in their own right, as their development must be coordinated with one other as well as the surrounding eye tissue, which is also undergoing development and growth.

Prior to the formation of scleral ossicles, we see the appearance of epithelial structures on the surface of the eye, the conjunctival papillae (Fig. 1). The papillae are outgrowths of the conjunctival epithelium which serve to induce the formation of the scleral ossicles in the mesenchyme below via an epithelial-mesenchymal signal (Pinto and Hall, 1991; Franz-Odenaal, 2008). Each papilla induces the formation of a single condensation (i.e., induction occurs in a 1:1 ratio; Coulombre et al., 1962). The growth of the papillae, and the induction of the underlying ossicles, occurs in a specific and well-conserved pattern. The first papilla to form does so at Hamburger and Hamilton stage 30 (HH 30) directly over the ciliary artery, and is designated papilla #12 (Coulombre et al., 1962; Franz-Odenaal, 2008). Development of papilla #12 is followed by the remainder of the temporal group (#10 -15), the nasal group (#2 -6), the dorsal group (#7-9) and finally papilla #1, which forms directly over the choroid fissure (Coulombre et al., 1962; Franz-Odenaal, 2008). A complete ring of papillae, typically containing 15 – 16 papillae per eye, is complete by HH 34 (Franz-Odenaal, 2008). Although the precise timeline of scleral ossicle induction remains contentious, induction is thought to occur over a period of 2-3 days beginning around HH 35 (Hall, 1981). Interestingly, the expression of alkaline phosphatase, an early marker of osteoblast differentiation, can be detected in the mesenchyme below papillae as early as HH 35 (Fig. 1B), suggesting either that induction begins before HH 35, or that mesenchymal cells respond to inducing signals very rapidly

(Wilson, 2014). Recent work from our lab has aimed at identifying key molecules involved in ossicle induction, and have identified sonic hedgehog (Franz-Odendaal, 2008), indian hedgehog (Duench and Franz-Odendaal, 2012) and bone morphogenetic protein 2 (Duench and Franz-Odendaal, 2012) as key players. Interestingly, *shh* and *bmp2* are expressed in the papillae in the same pattern in which the papillae form, suggesting that ossicle induction does not occur in unison but instead follows the same pattern in which the papillae form (Franz-Odendaal, 2008; Duench and Franz-Odendaal, 2012). Once induction is complete, papillae degenerate over a period of 1.5-2 days, and all papillae have disappeared by HH 38 (Franz-Odendaal, 2008).

The earliest histological sign of osteogenesis is the formation of a tightly clustered condensation in the deep scleral mesenchyme at HH 36.5 (Fig. 1C; note that the following description refers to the timeline by which condensation #12 forms; Franz-Odendaal, 2008; Jabalee et al., 2013). Condensed cells, likely preosteoblasts, begin to secrete a matrix rich in collagen I at this stage. As development proceeds, the condensed cells rearrange themselves into two distinct layers of osteoblasts separated by organic matter composed primarily of type I collagen fibers (osteoid). Secretion of osteoid serves to thicken the ossicles, which begin to mineralize at HH 39 (Franz-Odendaal, 2008; Zhang et al., 2012; Jabalee et al., 2013). Unlike the calvariae, which mineralize in a lateral to medial direction, mineralization of the scleral ossicles begins at their center and proceeds outwards toward their edges (Franz-Odendaal, 2011a). As ossicles approach one another they form areas of overlap which are similar in appearance to cranial sutures (Jabalee et al., 2013). Interestingly, when an ossicle fails to form, its neighbor often expands to fill the gap (Franz-Odendaal, 2008; Duench and Franz-Odendaal, 2012),

suggesting that the growth of each ossicle is regulated in part by interaction with the other ossicles in the ring. Once ossicles reach their final size, osteocytes undergo apoptosis, thereby preventing further remodeling of the bone (Palumbo et al., 2012). The fully formed sclerotic ring is thought to prevent distortion of the eyeball during corneal accommodation (Walls, 1942; Franz-Odenaal et al., 2007).

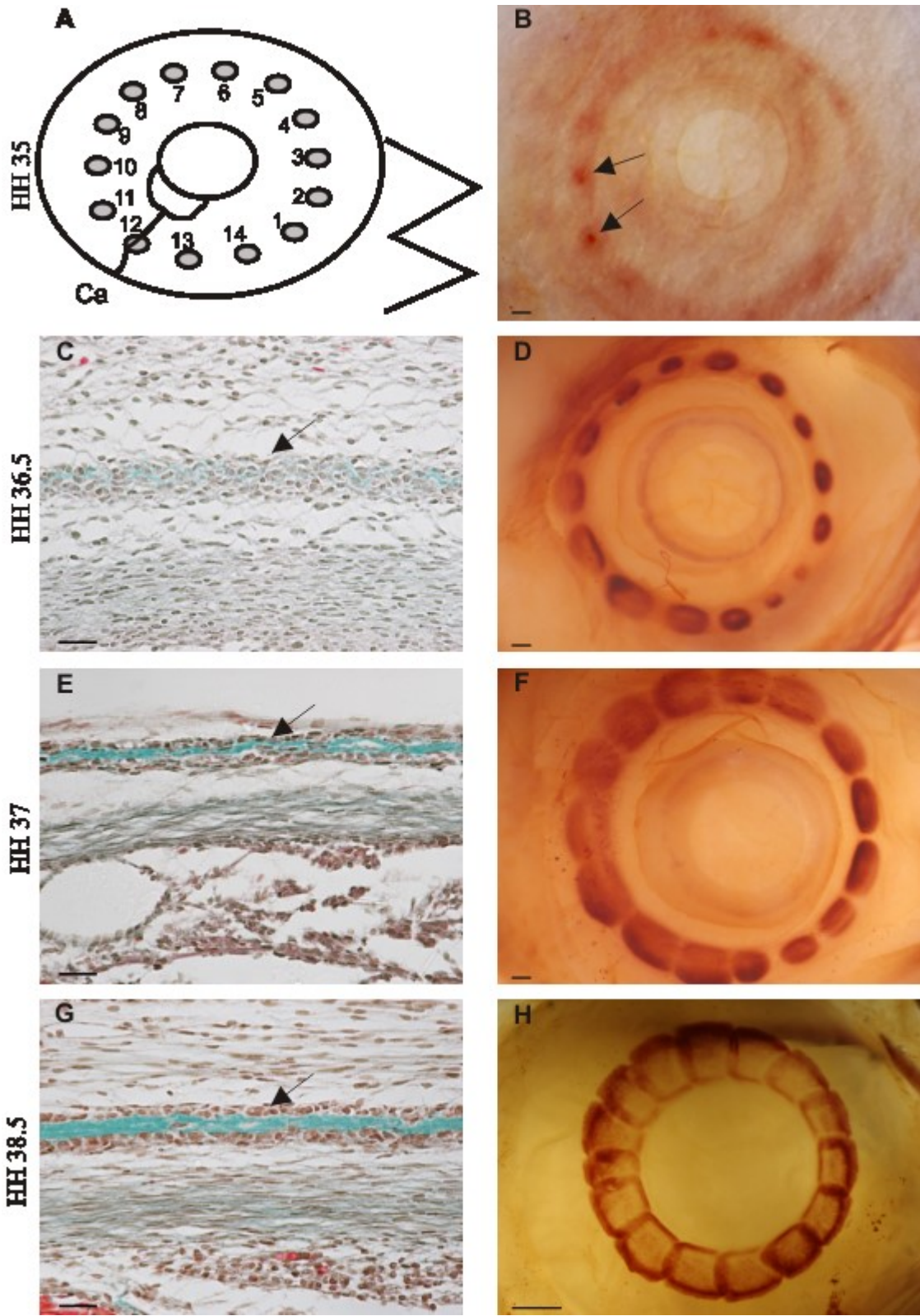


Fig. 1. Summary of scleral ossicle development from HH 35 - 38.5 (day 9 – 12.5). (A) A schematic summarizing the major landmarks of the eye at HH 35. All figures throughout this thesis are shown in this orientation with the beak to the right and the ciliary artery left, ventral. Papillae are numbered according to their position around the eye, with papilla #12 always over the ciliary artery (Ca). (B) Alkaline phosphatase (AP) staining at HH 35. AP is expressed weakly in the temporal group papillae (arrows) and mesenchyme. (C) Histological section stained with Masson's trichrome at HH 36.5. The condensation (arrow) is visible as a dense cluster of cells. (D) AP staining at HH 36.5 indicates that osteoblast differentiation is underway in all ossicles at this stage. (E) Histological section at HH 37. The condensation (arrow) has become more organized, with a layer of osteoblasts surrounding a thick layer of osteoid (green). (F) AP staining at HH 37 reveals a ring of enlarged condensations. Each is distinct and does not overlap its neighbor. (G) Histological section at HH 38.5. A mature condensation (arrow) is present consisting of a thick layer of osteoid surrounded on each side by multiple layers of osteoblasts. (H) AP staining at HH 38.5 reveals that condensations continue to expand, eventually overlapping one another and mineralizing. Scale bars: 20 μm in C, E, G; 1000 μm in B, D, F, H. Histological figures (C, E, G) are adapted from Jabalee et al. (2013).

1.4 The Role of Vasculature in Bone Development

Adult bone is highly metabolic and requires a great degree of vascularization in order to function properly. However, during development blood vessels do much more than simply provide metabolic support to skeletal cells; instead, they appear to play an active role in regulating bone cell activities. This intimate relationship between bone and vasculature, though poorly understood, is absolutely required for proper formation of a mature skeletal element.

Here I will examine the broad features of the relationship between skeletal cells and vasculature during development, and discuss the implications of these observations for the understanding of bone development. Although the focus of my studies is on intramembranous flat bones of the skull, the majority of the literature is concerned with development of the endochondral long bones of the limb. Thus, our limited knowledge of the skull will be supplemented with a much deeper, though still largely incomplete, examination of the relationship between vasculature and the limb skeleton.

The relationship between vasculature and the skeleton begins as early as the condensation phase of skeletal development. Regardless of the type of bone formed (intramembranous versus endochondral), condensations form in areas completely devoid of vasculature (Thompson et al., 1989; Eshkar-Oren et al., 2009; Jourdeuil and Franz-Odenaal, 2012). Such areas are termed avascular zones. In the mouse limb, avascular zones are formed via regression of existing vessels, and this regression occurs before condensations begin to form (Eshkar-Oren et al., 2009). In contrast, camera lucida drawings of the scleral vasculature of the chick eye suggest that avascular zones which surround the intramembranous scleral ossicles are not formed by regression, as these

areas are not vascularized in the first place (Jourdeuil and Franz-Odenaal, 2012).

Additionally, obliteration of the avascular zone surrounding the condensation of digit 2 in the chick limb results in failure of the cartilage element to form, suggesting that avascular zones are required for subsequent chondrogenesis (Yin and Pacifici, 2001).

Avascular zones are low in oxygen, a condition known as hypoxia (Amarilio et al., 2007). Through stabilization of hypoxia inducible transcription factors (Hifs), hypoxia results in widespread changes in gene expression which alter such diverse cellular processes as proliferation, apoptosis, glucose metabolism and the regulation of angiogenesis (Carroll and Ashcroft, 2005). Mice deficient in Hif-1 display severely undermineralized limb bones with abnormal joints (Amarilio et al., 2007; Provot et al., 2007), whereas constitutive activation of Hif-1 during distraction osteogenesis results in increased bone vascularity and accelerated bone repair (Wan et al., 2008). These results suggest that Hifs play an essential role in bone formation in both embryonic and adult mice. The mechanism by which Hif-1 promotes bone formation is unknown, but it appears to be required for such diverse processes as chondrocyte survival (Schipani et al., 2001; Maes et al., 2012), collagen synthesis under hypoxic conditions (Bentovim and Zelzer, 2012), and the expression of *sox9*, a master regulator of chondrocyte differentiation (Amarilio et al., 2007). Although the role of Hifs during development of intramembranous skull bones has not been explicitly examined, Hifs have been shown to play a key role in the regulation of cranial neural crest cell migration (Barriga et al., 2013), a process essential to the development of the anterior skull bones. Furthermore, osteoblasts of the pig mandible (an intramembranous bone) have been shown to express

hif-2, but not *hif-1* (De Spiegelaere et al., 2010), suggesting that alternative regulatory pathways may be at work in intramembranous bones compared to endochondral ones.

In addition to the factors described above, Hifs are well known for their ability to regulate angiogenesis, the growth and branching of blood vessels, via the expression of vascular endothelial growth factor A (*vegfa*). Given the extreme importance of this gene to the remainder of this thesis, a brief discussion of its basic biology is warranted. *Vegfa* is capable of giving rise to a number of splice variants via the process of alternative splicing (reviewed in Robinson and Stringer, 2001). These splice variants are named according to the number of amino acids in the final form of the protein (e.g. Vegf_{121} , Vegf_{164}). Chickens contain at least 4 splice variants which differ from their human counterparts by two amino acids (Schmidt and Flamme, 1998; Fig. 2a). Once secreted, each splice variant displays different properties; for instance, approximately 50-70% of secreted Vegf_{165} remains bound to the cell surface or to components of the extracellular matrix, probably due to its slight affinity for heparan sulphate proteoglycans (HSPGs), whereas Vegf_{121} diffuses freely and is not bound by HSPGs (Robinson and Stringer, 2001). ECM-bound Vegf molecules may act as a reservoir of growth factor, whereas freely diffusing Vegf molecules interact directly with endothelial cells by binding one of two major receptors (Vegfr-1, also called fms-like tyrosine kinase-1 or Flt-1, and Vegfr-2, also called fetal liver kinase-1 or Flk-1) or the co-receptor neuropilin-1 (Robinson and Stringer, 2001). Vegfr-1 and 2 are required for proper vascular patterning during early development (Robinson and Stringer, 2001). Interestingly, Vegfr-1 has a higher affinity for Vegf than does Vegfr-2, but is less efficient at transducing the signal to the interior of the cell (Shibuya, 2001; Fig. 2b). Furthermore, alternative splicing of Vegfr-1 can give

rise to a truncated, secreted form of the receptor, termed sFlt-1, which has antiangiogenic properties *in vitro* and *in vivo* (Shibuya, 2001; Robinson and Stringer, 2001; Yamaguchi et al., 2002). The co-receptor neuropilin 1 (Nrp1) interacts specifically with Vegf₁₆₅ and increases its ability to signal through Vegfr-2; knockdown studies have revealed that, like the major receptors, Nrp1 is required for proper vascular patterning during early development (Robinson and Stringer, 2001).

A

<u>Human</u>	<u>Mouse</u>	<u>Chick</u>
Vegf121	Vegf120	Vegf122
Vegf145	Vegf144	Vegf146
Vegf165	Vegf164	Vegf166
Vegf189	Vegf188	Vegf190
Vegf206	Vegf205	

B

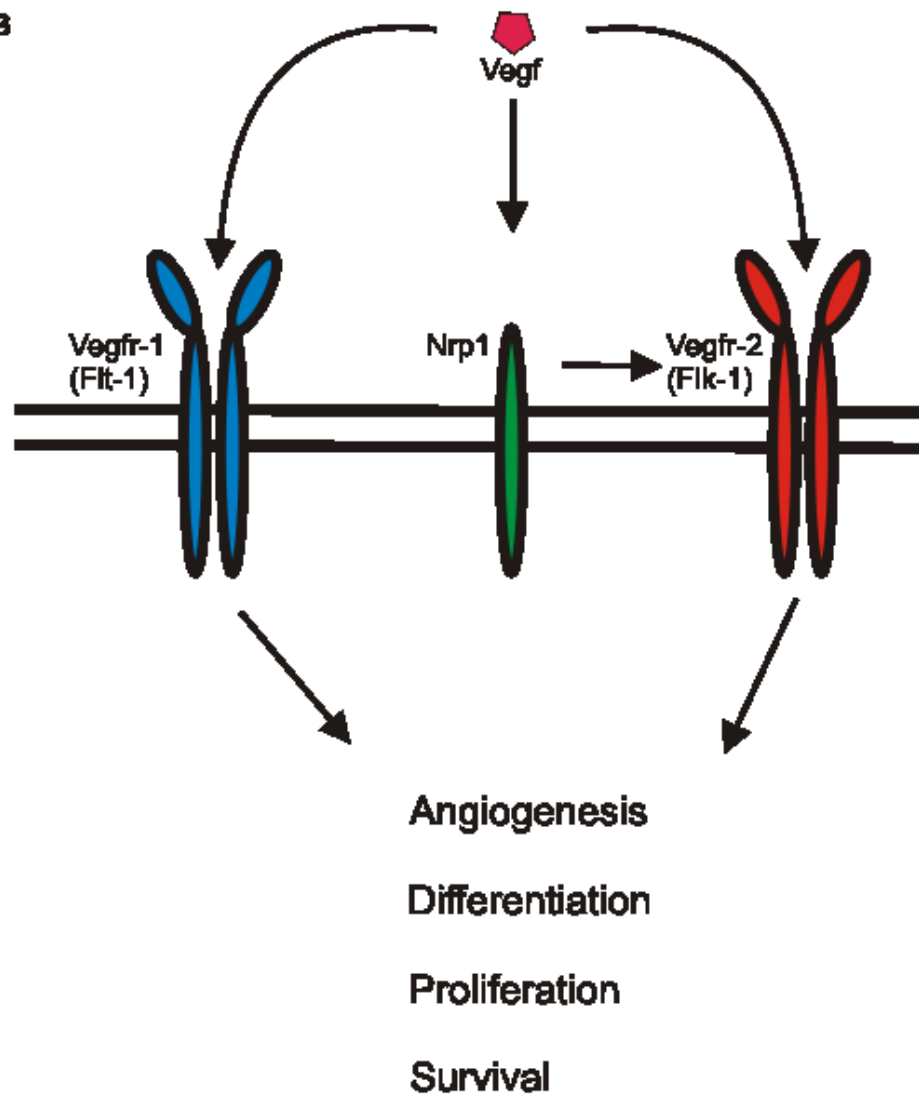


Fig. 2 Vegf signaling. (A) Summary of the *vegfa* splice variants found in human, chick and mouse. (B) Diagram illustrating the Vegf signaling cascade. Vegf signals through two receptors designated Vegfr-1 (Flt-1) and Vegfr-2 (Flk-1). The co-receptor neuropilin-1 interacts specifically with the Vegf₁₆₅ splice variant, increasing its signaling through Vegfr-2. Vegf signaling results in a number of cellular effects, including increased angiogenesis, differentiation, proliferation and survival.

Vegfa is expressed diffusely throughout the early mouse limb bud, but later becomes restricted to the chondrocytes of the limb skeleton and eventually to the hypertrophic zone of each cartilage element, where blood vessel invasion and endochondral ossification will occur (Eshkar-Oren et al., 2009). Mutant mice which express only Vegf₁₂₀, and lack the other five isoforms (termed Vegf^{120/120}), display poor vascularization, delayed endochondral ossification, and undermineralization of both limb and calvarial bones (Zelzer et al., 2002). Interestingly, expression of *vegfa* by hypertrophic chondrocytes requires Runx2 (Zelzer et al., 2001), thought to be a master regulator of osteoblast differentiation. Runx2 deficient mice show a severe delay in endochondral ossification similar to that observed in Vegf^{120/120} mice (Zelzer et al., 2001). Thus, it is clear that Vegf plays a key role in promoting the proper vascularization of developing bone tissue.

Blood vessels which invade the hypertrophic zone of the developing cartilage serve to deliver osteoprogenitors to what is now called the primary ossification center (Maes et al., 2010). These cells, along with osteoprogenitors arising in the periosteal connective tissue immediately surrounding the bone, must differentiate into mature osteoblasts prior to depositing bone tissue on the degraded cartilage anlagen. Interestingly, the process of osteoblast differentiation is tightly linked to the process of vascular invasion and appears to require Vegf. For instance, addition of exogenous Vegf to the growth medium of calvaria-derived and bone marrow-derived cultures has been linked to increases in alkaline phosphatase production (Midy and Plouet, 1994), osteoblast migration and proliferation (Midy and Plouet, 1994; Mayr-Wohlfart et al., 2002), and mineralization (Deckers et al., 2000; Mayer et al., 2005). Additionally,

conditional knockout of *vegfa* in *osterix*-expressing cells (i.e. osteoblast lineage cells) results in the formation of thin long bones with a significantly greater number of adipocytes in the bone marrow cavity compared to wild type littermates (Liu et al., 2012). These intriguing results suggest that Vegf plays a role in the determination of cell fate; wild type levels of Vegf tip the scale towards osteoblastogenesis, whereas an absence of Vegf tips the scale towards adipocytogenesis. Perhaps even more intriguing is the observation that the addition of exogenous Vegf to cultures of bone marrow cells derived from mutant mice does not return the balance of differentiation toward osteoblasts (Liu et al., 2012), suggesting that Vegf plays an intracrine role within mesenchymal stem cells which is distinct from its paracrine effects on nearby endothelial cells.

Vegf likely promotes osteoblast differentiation during development of the calvariae as well. $Vegf^{120/120}$ mice show poor vascularization and undermineralization of the calvariae (Zelzer et al., 2002), though this phenotype appears less severe than that of the limb bones. Further evidence for the importance of Vegf during intramembranous ossification comes from studies of distraction osteogenesis. Regardless of the area of surgery, the majority of new bone is formed via intramembranous ossification (although small amounts of cartilage may form as well; Jacobsen et al., 2008). *Vegfa* and its receptors are expressed by the cells of the distraction gap shortly after surgery and expression persists throughout fracture repair (Pacicca et al., 2003; Byun et al., 2006). Inhibition of Vegf signaling by application of a neutralizing antibody toward Vegfr-1, Vegfr-2, or both results in a decrease in vascularization of the distraction gap as well as a significant reduction in new bone formation due to a lack of skeletal cells (Jacobsen et al., 2008).

The above experiments serve to highlight the importance, and the complexity, of the interaction between skeletal cells and blood vessels during osteogenesis. Though great strides have been made in recent years to understand the importance of this interaction during endochondral ossification, studies of intramembranous bones have lagged behind. Furthermore, those studies focusing on intramembranous bones tend to be performed in culture or in experimental models, such as distraction osteogenesis, which may not recapitulate the events of development. Thus, in-depth studies of the role of vasculature during normal embryonic development of intramembranous bones are clearly required to elucidate the role of vasculature in intramembranous ossification *in vivo*.

1.5 Hypotheses and Objectives

Based on observations of the key role of vasculature during endochondral ossification I hypothesise that:

1. Growth of the scleral vasculature and the formation of the scleral ossicles are coordinated with one another.
2. Vegf is expressed during scleral osteogenesis and links vascular growth to intramembranous bone development.

The objectives of this research are, in a broad sense, to better understand the relationship between vasculature and developing intramembranous bones using an *in vivo* model, the scleral ossicles of the chick. More specific objectives are as follows:

1. To map the development of vasculature in relation to scleral ossicle development.
2. To determine the spatiotemporal expression pattern of *vegfa* during scleral ossicle development.

3. To determine the role of the papilla, if any, in patterning scleral vasculature.
4. To determine the role of Vegf, if any, in early ossicle development.

Chapter 2.0: Materials and Methods

2.1 Chicken Embryos

Fertilized White Leghorn (*Gallus gallus*) eggs were obtained from the Nova Scotia Agricultural College (Truro, NS) or Cox Brothers Farm (Truro, NS) depending on availability. Eggs were incubated at $37 \pm 1^\circ\text{C}$, 40% humidity and were turned 1-2 times daily. Chicken embryos were staged according to the Hamburger and Hamilton (1951) staging series.

In order to gain access to the embryo for manipulation, a small window was made in the shell of embryos destined for bead implantation or ink injection as follows. On the third day of incubation, a small hole was made at the apex of the egg through which 5-6 ml albumin was removed using a sterile needle. With the egg lying horizontally, a second small hole, approximately 5-10 mm in diameter, was then made, thereby granting access to the embryo. Forty microliters penicillin-streptomycin (5000 units penicillin, 5 mg/ml streptomycin; Sigma, P4458) was applied to the albumin of each embryo to aid in preventive post-operative infection. All holes in the shell were then sealed with Scotch tape and the embryos incubated until the desired stage.

2.2 Blood Vessel Visualization using Spotliter Highlighter Ink

2.2.1 Preparation of Microcapillary Pipettes

Microcapillary pipettes (Sutter Instrument Co., BF100-50-10) were pulled using a Flaming/Brown micropipette puller (Sutter Instrument Co., Model P-97). This resulted in an extremely fine tip capable of piercing blood vessels without causing excessive bleeding.

2.2.2 Preparation of Ink

In order to visualize the scleral vasculature, ink from yellow Pilot Spotlitter brand highlighter pens was injected into the vitelline artery prior to embryo fixation. Highlighter ink has been shown to fluoresce dramatically when used with green fluorescent protein (GFP) and cyanine 3 (Cy3) filters and to out-perform more commonly used substances such as fluorescein isothiocyanate (FITC)-labeled dextran at the task of blood vessel visualization in whole-mount chick and mouse embryos (Takase et al., 2013). The ink-soaked felt was removed from yellow Spotlitter highlighter pens and placed in 10 ml 1x PBS. The felt was agitated to cause release of ink until the solution was saturated. This process could be repeated with multiple 10 ml aliquots of PBS, resulting in 20 – 30 ml injectable ink per highlighter.

2.2.3 Ink Injection

Access to windowed embryos was gained by removal of the overlying tape. The ink (7.5 μ l/dose) was injected into the vitelline artery using a pulled glass micropipette inserted into a mouth pipette. Embryos were then incubated for 10 minutes at 37°C to allow ink to circulate, decapitated, fixed overnight in 4% PFA at 4°C and stored in 1x PBS. Fluorescent images were obtained using a Nikon SMX 1500 microscope with a Nikon Intensilight C-HGFI illuminator. Images were captured using a Nikon camera and NIS Elements software package.

2. 3 Probe Preparation, Whole Mount In Situ Hybridization and Cryosectioning

2.3.1 Molecular Cloning

Plasmid containing an 843 base pair portion of the *Gallus gallus vegfa* coding region (GenBank Accession Number BU269995) was a kind gift from Dr. Todd Camenisch (College of Pharmacy, University of Arizona). Plasmid was removed from filter paper by incubating in TE buffer (10 mM Tris-Cl, 1 mM EDTA, pH 8.0) for 5 minutes at room temperature. The sample was agitated briefly using a vortex mixer and centrifuged for 1 minute at 3000 rpm. The sample was then incubated for 30 minutes at room temperature and the filter paper was removed prior to storing at -20°C.

E. coli cells (HB101 competent cells, Promega, L1011) were transformed with plasmid as follows: 100 µl of competent *E. coli* cells was added to each of two chilled Nalgene tubes using chilled pipette tips. To the experimental tube, 10 µl *vegfa* plasmid was added; to the control tube, 10 µl TE buffer. Each tube was chilled on ice for 15 minutes, heat shocked at 42°C for 45 seconds and chilled on ice for an additional 2 minutes. Nine hundred microliters cold Luria-Bertani (LB; Becton, Dickinson and Company, 244620) broth was added to each of the two tubes, which were then incubated at 37°C for 1 hour with gentle shaking (45 rpm). LB agar plates containing 0.01% ampicillin trihydrate (Sigma, A6140) were placed in the incubator upside down to warm during this time. Ten and 100 µl volumes of broth/plasmid-transformed cell mixture were then spread onto agar plates using sterile technique and incubated overnight at 37°C. One hundred microliters broth/TE-transformed cell mixture was plated as a control. Since the plasmid contains an ampicillin resistance gene, only cells which have been successfully transformed are able to grow.

The following day, experimental plates had well-defined bacterial colonies whereas control plates lacked bacterial growth as expected. Using sterile technique, a small amount of LB broth was poured into a Nalgene tube. A sterile pipette tip was used to remove a single colony from the 100 μ l experimental plate and the tip was placed into the tube containing LB broth. The tube was incubated overnight at 37°C.

2.3.2 Isolation of Plasmid DNA

Minipreparation was performed to isolate plasmid DNA as follows. Two milliliters LB broth containing transformed *E. coli* cells was placed in a 2 ml Eppendorf tube and centrifuged for one minute at maximum speed (13000 times gravity) causing bacterial cells to form a pellet in the bottom of the tube. The process was repeated with a second 2 ml volume of cells to increase yield; the supernatant was discarded. Two hundred and fifty microliters cold buffer #1 (100 μ g/ml ribonuclease A (Sigma, R-4642), 50 mM Tris-Cl, 10 mM EDTA, pH 8.0) was added to the tube which was then dragged across a tube rack 10 times to re-suspend the pellet. Cold lysis buffer (0.2 M NaCl, 1% SDS) was then added to the tube, which was inverted three times to mix and chilled on ice for five minutes in order to break open bacterial cells. Addition of 250 μ l cold potassium acetate (Sigma, P1191) caused chromosomal DNA, proteins and lipids to precipitate, turning the solution cloudy. The tube was inverted three times to mix, chilled on ice for five minutes and centrifuged at max speed for five minutes. Supernatant was put in a fresh tube; pellet was discarded. Two hundred microliters phenol-chloroform was added and the tube was shaken vigorously for 30 seconds. The tube was centrifuged at max speed for five minutes, causing the solution to separate into two layers. The top layer

was carefully removed and placed in a fresh tube; the bottom layer was discarded. An equal volume of isopropanol was added and the tube was mixed by inversion for 30 seconds. The sample was incubated at room temperature for two minutes, centrifuged at max speed for five minutes and the resulting supernatant was discarded. A white pellet was visible in the bottom of the tube. The pellet was allowed to dry at room temperature for 15 minutes before re-suspending in 50 μ l of 0.01% diethyl pyrocarbonate-treated water (DEPC H₂O).

2.3.3 *Linearization of vegfa cDNA*

Plasmids were engineered to contain endonuclease restriction sites which can be cut by specific enzymes, resulting in linearization of the circular plasmid. (Depending on the enzyme used, the resulting linearized cDNA may be used to produce either antisense probe or sense probe). Linearization was performed by combining 5 μ l *vegfa* cDNA (from minipreparation, see section 2.2.2), 5 μ l restriction enzyme, 10 μ l buffer, 10 μ l bovine serum albumin (BSA; New England Biolabs, B90015) and 70 μ l DEPC H₂O. NotI (New England Biolabs, R01895) in buffer 3 (New England Biolabs, B70035) was used to produce linearized antisense cDNA; SalI (Promega, R605A) in buffer D (Promega, R004A) was used to produce linearized sense cDNA. (Each buffer is specific to, and comes with, the corresponding restriction enzyme). Reagents were incubated at 37 °C overnight by placing tubes in a Mastercycler personal PCR machine (Eppendorf, 5332). The reaction was stopped by heat inactivation at 65°C for 15 minutes.

2.3.4 Purification of Linearized *vegfa* cDNA

Purification of linearized cDNA was performed using a High Pure PCR product purification kit (Roche, 11 732 668 001, version 16) according to the manufacturer's instructions. Briefly, digested (linearized) *vegfa* cDNA was combined with 500 μ l binding buffer and centrifuged at max speed for 1 minute. This allows cDNA to bind to the High Pure Spin filter (containing glass fiber fleece) while contaminants are discarded in the flowthrough. The filter was rinsed with wash buffer and centrifuged to further remove contaminants. The filter was then rinsed with elution buffer, which removes the DNA from the filter. Two eluates were collected for each sample (i.e. NotI digested and Sall digested).

2.3.5 Gel Electrophoresis

cDNA before and after purification (2 μ l/sample) were separately combined with 6x load dye (Promega, G190A) and loaded onto a 1.5% agarose gel in 1xTBE (89 mM Tris-Cl, 89 mM boric acid, 2 mM EDTA, pH 8.0) containing 3X GelRed nucleic acid gel stain (Biotium, 41003). A 1 kb ladder (Promega, G694A) was used to determine the approximate size and concentration of samples (the brightest band of ladder represents approx. 1 μ g/ μ l). Electrophoresis was performed at 120 V for 1 hour. The gel was imaged using AlphaImager and results were used to estimate cDNA concentration.

2.3.6 Probe Synthesis

Purified *vegfa* cDNA was used to create a digoxigenin (DIG)-labeled RNA probe using a DIG-RNA labeling kit (Roche, 11 175 025 910) according to the manufacturer's

instructions. Briefly, 1 μg purified *vegfa* cDNA was combined with 2 μl DIG-RNA labeling mix, 2 μl 10x transcription buffer, 1 μl protector ribonuclease (RNase) inhibitor, 2 μl enzyme [T3 polymerase (Roche, 11 031163 001) or T7 polymerase (Roche, 10 881 767 001) for synthesis of antisense or sense probe, respectively] and DEPC H₂O to a final volume of 20 μl . The mixture was incubated at 37°C for 2 hours in a Mastercycler PCR machine. Two microliters of DNase I (Roche, 04 716 728 001) was added to the mixture to degrade *vegfa* cDNA, leaving only RNA intact. The tube was returned to the PCR machine at 37°C for 15 minutes. The reaction was stopped by addition of 2 μl 0.2 M EDTA (pH 8.0). Probe was stored at -20°C until required.

A dot blot was used to estimate RNA probe concentration and DIG-labeling efficiency, as suggested by the DIG-RNA labeling protocol. One microliter of each sense and antisense probe, as well as control RNA provided in the kit, were used to make a dilution series consisting of five concentrations of probe (1 ng/ μl , 10 pg/ μl , 3 pg/ μl , 1 pg/ μl and 0.3 pg/ μl). One microliter from each concentration was then dotted onto a nitrocellulose membrane (Roche, 11 209 299 001), which was baked at 120°C for 30 minutes to prevent loss of nucleic acid during subsequent steps. The membrane was then incubated in maleic acid buffer (0.1 M maleic acid, 0.15 M NaCl) for two minutes, placed into blocking buffer (2% sheep serum, 3% skim milk powder in 1xTBST) for 20 minutes, briefly washed in 1x TBST and incubated in antibody solution [1:5000 anti-DIG-AP antibody (Roche, 11 093 274 910) in 1x TBST] for 30 minutes at room temperature with gentle shaking. The membrane was then placed in washing buffer (0.1 M maleic acid, 0.15 M NaCl, 0.3% TWEEN 20) briefly before incubation in detection buffer (0.1 M Tris-Cl, 0.1 M NaCl, pH 8.0). Incubation in color detection buffer (0.15 mg/ml BCIP,

0.30 mg/ml NBT) was conducted in the dark at room temperature and the membrane was examined periodically for the appearance of color over the course of one hour. If probes develop color in a similar time frame and intensity to control RNA then the DIG-labeling process was considered successful.

2.3.7 Whole Mount *In Situ* Hybridization

Whole mount *in situ* hybridization was used in order to determine the spatiotemporal expression pattern of *vegfa*. The protocol was adapted from that of Nieto et al. (1996) and Franz-Odenaal (2008) with modification. A detailed version of the protocol, including recipes for solutions, can be found in Appendix F.

Embryos were decapitated and placed in 1x PBST for staging according to Hamburger and Hamilton (1951). Heads were then fixed in 4% PFA/1x PBST overnight at 4°C and dehydrated through a graded methanol series. Heads were stored in 100% methanol at -20°C for at least 24 hours before continuing with processing. Heads were bisected sagittally in cold 100% methanol and the vitreous humor and lens were removed through a hole in the back of the eye prior to rehydration through a graded methanol series. Half heads were bleached overnight in 10% hydrogen peroxide to remove eye pigment, permeabilized in 50 µg/ml proteinase K, post-fixed in 2% PFA/0.25 % glutaraldehyde in 1x PBST and incubated in prehybridization buffer (prehyb) before hybridization with 2.5 ml prehyb containing 2 µl probe overnight at 60°C with gentle shaking.

The next day, half heads were rinsed in prehyb to remove unbound probe and placed in blocking solution (20% sheep serum in 1xTBST, heat inactivated) before

incubation in the anti-DIG antibody solution [1:10, 000 anti-DIG-AP antibody, preabsorbed with chick powder to increase specificity (see Appendix F), in blocking solution] overnight at 4°C. Samples were washed to remove excess antibody and incubated in 1x TBST containing 2mM levamisole for two to four days to remove endogenous alkaline phosphatase activity and reduce background. Half heads were then rinsed in 1x NTMT and placed in color detection [1 SIGMAFAST BCIP/NBT tablet (Sigma, B5655) per 10 ml 1x NTMT with 10% polyvinyl alcohol (PVA; Sigma, 348406)] in the dark. For embryos older than HH 36.5, the anterior of the eye was removed from the head prior to incubation in color detection. The color reaction was stopped by incubating samples in 1x PBST containing 5 mM EDTA. Half heads were post-fixed in 4% PFA in 1x PBST. Following post-fixation, the anterior of each eye was dissected and the retinal pigmented epithelium (RPE) and neural retina were removed. Background was leached in 90% methanol. Samples were stored in 50% glycerol/water mix at 4°C in the dark.

In addition to treatment with antisense probe, some half heads received either sense probe or no probe as negative controls. Because the sense probe does not specifically bind the *vegfa* transcript, it is used to measure the level of non-specific binding which occurs inevitably for all probes and can provide an estimate of background levels. Controls in which probe was excluded test for non-specific binding and trapping of the antibody, as well as for possible cross-contamination between samples which may occur during processing. Three to five half-heads were reacted with antisense probe at each stage examined.

2.3.8 Cryosectioning of In Situ-Stained Embryos

In order to determine the location of *vegfa* expression in detail, *in situ*-stained tissues were cryosectioned as follows. A small piece of eye tissue containing either a single papilla of the nasal group and half of the interpapillary tissue on either side (HH 35 and HH 36.5) or a condensation and half of the condensation on either side (HH 37.5, HH 38.5) was dissected from the eyes of *in situ*-stained samples and rinsed in distilled water for 15 minutes to remove glycerol. A 1% agar solution was poured into a small plastic Petri dish and allowed to cool for 2 – 3 minutes. The dissected sample was blotted to remove excess water and placed in the molten agar which was allowed to harden for at least 10 minutes at 4°C. The hardened agar was trimmed to form a small, rectangular block containing the embedded tissue. The block was soaked in 30% sucrose until it had sunk; typically, this requires allowing it to soak overnight. Prior to sectioning, the block was attached to a chuck using Jung Tissue Freezing Medium (Leica Microsystems, 0201 08926). Sections were cut at 10 - 12 µm thickness at a temperature between – 24 and – 26°C in a Leica CM1850 cryostat and collected on (3-aminopropyl)triethoxysilane (APTES)-coated slides (Appendix G). Slides were coverslipped using Gel Mount aqueous mounting medium (Sigma, G0918) according to the manufacturer's instructions and viewed using a Nikon Eclipse 50i compound microscope.

2.4 Vegf Inhibitor Application

2.4.1 Preparation of Vegf Inhibitor

A soluble form of Vegfr-1, known as soluble fms-like tyrosine kinase 1 (sFlt-1), has been shown to exhibit antiangiogenic properties by binding and inactivating all

isoforms of extracellular Vegf in mammals (Kendall et al., 1996) and in avians (Yamaguchi et al., 2002). Lyophilized sFlt-1 (R&D Systems, 321-FL-050/CF) was reconstituted at 100 µg/ml in sterile 1x PBS, aliquoted and stored at -20°C. sFlt-1 has been shown to inhibit the formation of new blood vessels while having no discernable effect on pre-existing vessels in chick and quail embryos *in vitro* and *in vivo* (Argraves et al., 2002).

2.4.2 Preparation of Beads for Implantation

Affi-gel blue agarose beads (Bio-Rad, 153-7302), approximately 60 – 80 µm in diameter, were pre-washed in sterile 1x PBS before use as follows. Beads were placed in an Eppendorf tube containing sterile 1x PBS. The tube was centrifuged at 13,000 rpm for one minute to collect beads at the bottom of the tube. The PBS was then removed and replaced with fresh 1x PBS. The whole process was repeated to ensure complete removal of storage solution from the beads. Beads were stored at 4°C until required.

On the day of the implantation, PBS was removed and beads were allowed to dry completely (until shrivelled). To do this, Parafilm was used to cover the inside surface of a small Petri dish. The cap of a small Eppendorf tube was broken off and affixed to the Parafilm. Beads in 1x PBS were placed in the cap, and PBS was removed. Control and experimental beads were prepared by application of 25 µl of 1x PBS or sFlt-1 (100 µg/ml), respectively, immediately prior to the beginning of implantation. Beads were kept on ice throughout the experiment.

2.4.3 Preparation of Tungsten Needles

Fine (0.1 mm) and blunt (0.25 mm) tungsten needles were used for fine manipulations. Glass pipettes were flamed to soften the glass and pulled to produce a long, narrow tip. A diamond knife was used to etch the base of the tip, resulting in a small hole through which tungsten wire was threaded. The hole was then flamed again, causing the glass to melt around the wire, holding it in place. Needles were electrolytically sharpened as follows. Two crocodile clips (the electrodes) were attached to a power supply. One electrode was attached to a metal paper clip which was partially submerged in 1 N NaOH while the other electrode was submerged in the same NaOH and placed into contact with the region of the needle to be sharpened. Application of an electric current results in electrolysis of the tungsten and sharpening of the needle (Brady, 1965).

2.4.4 Membrane Dissection

By HH 34, embryos are covered by the highly vascular chorioallantoic membrane (CAM). Tearing of the CAM vasculature, a requirement to gain access to the eye at stages greater than HH 34, is the main cause of embryo death following bead implantation. In order to improve access to the eye and prevent tearing CAM vasculature, membranes were dissected two days prior to bead implantation, at HH 33. At this stage, the CAM remains open near the posterior of the embryo. The opening was torn using fine forceps. The edge of the CAM was then gently separated from the underlying yolk sac by tearing the thin, avascular membrane which connects them. This prevents the CAM from sealing over before the day of implantation, allowing the surgery to be performed without tearing of CAM vasculature.

2.4.5 Bead Implantation

Access to HH 35 embryos (see section 2.1) was gained by removal of the overlying tape. Fine forceps were used to carefully reposition the embryo so that the head lay in the hole in the CAM which was created two days prior (see section 2.3.4). The amniotic membrane, which is mostly avascular, was torn when necessary. A fine tungsten needle was used to create a small nick in the conjunctival epithelium and a small epithelial slit was made adjacent to a papilla. The precise papilla targeted was determined by the orientation of the embryo and was carefully noted. The temporal, nasal and dorsal groups received approximately equal numbers of implantations. Beads were transferred onto the eye and tucked into the epithelial slit using sterile forceps or a blunt tungsten needle. Embryos were treated with 40 μ l penicillin-streptomycin (Sigma, P4458), sealed with Scotch tape and incubated at 37°C for an additional 24-48 hours.

2.4.6 Statistical Analysis

Embryos were injected with yellow Spotlter ink (see section 2.2) and fixed in 4% PFA one or two days post-surgery (dps). The anterior half of each eye was dissected, flat mounted and fluorescent images were obtained using a Nikon SMX 1500 microscope with a Nikon Intensilight C-HGFI illuminator. The area tool in NIS Elements (Nikon Software, BR 3.00) was used to carefully outline avascular zones (see Fig. 8A, B for an example). The size of the avascular zone surrounding the bead was measured three times per eye, and the average of the measurements was taken to reduce measuring error. The procedure was repeated for the avascular zone surrounding the equivalent papilla of the contralateral eye of each embryo. The difference in area between the implanted and

unimplanted eyes was found for each of eleven sFlt-1 implants and three 1x PBS controls at 1 dps. A constant was added to each difference in order to make all values positive, and the square root of each value was taken in order to normalize the data. An average was calculated for each group (sFlt-1 versus 1x PBS) and statistical significance was calculated using an independent two-sample Student's *t*-test (Minitab version 14). Raw data is shown in Appendix H.

2.4.7 Alkaline Phosphatase Staining

Alkaline phosphatase is an enzyme produced by a number of cell types including preosteoblasts and osteoblasts, thereby making it a useful indicator of early osteoblast differentiation and activity. Alkaline phosphatase was detected by an enzymatic assay according to the protocol of Edsall and Franz-Odenaal (2010). Briefly, fixed tissues were washed in distilled water and equilibrated in tris-maleate buffer [2.4% tris, 2.2% maleic acid (Fisher Scientific, 03417); pH 8.3] for one hour prior to detection of enzyme activity via reaction with AP substrate solution [1 mg/ml naphthol AS-TR phosphate (Sigma, N6125), 1% N,N-dimethylformamide (Sigma, 319937), 0.08% Fast Blue B salt (Sigma, D9805) in tris-maleate buffer] to produce a colored precipitate. Embryos were rinsed in saturated sodium borate water to stop the reaction, bleached overnight in 0.3% H₂O₂/1% KOH and processed through a graded glycerol series ending in 80% glycerol in 1% KOH.

Chapter 3.0: Results

3.1 Mapping the Growth of Scleral Vasculature

Previous studies from our lab have used camera lucida drawings and erythrocyte autofluorescence in order to map the early formation of the scleral vasculature of the embryonic chick from HH 28 – 36.5 (Jourdeuil and Franz-Odenaal, 2012). However, these techniques exhibit low resolution, particularly at advanced stages when a dense vascular meshwork is present. In order to map the development of vasculature in relation to scleral ossicle development more precisely, I injected yellow Spotlitter highlighter ink into the vasculature of the embryonic chick (Takase et al., 2013) from HH 35 – 38, the timeline over which the major events of scleral ossicle development occur.

The vascular meshwork of the sclera is first visible at early HH 35 (Fig. 3A). At this stage, vasculature, located in the superficial mesenchyme, is seen to approach and quickly surround the posterior papillae (i.e. those of the temporal group, which are the first to appear), which form from the overlying conjunctival epithelium. Distinct avascular zones form around these papillae, as previously described (Jourdeuil and Franz-Odenaal, 2012; Fig. 3A'). Avascular zones are large at first, but become smaller over the course of approximately 12 - 36 hours until they are eventually abolished. The anterior of the eye in the region of the conjunctival papillae remains avascular at this stage (Fig. 3A'').

By HH 36 the vascular network of the sclera has been well established (Fig. 3B). At this time the temporal papillae are no longer surrounded by avascular zones and the vascular meshwork in this region has become dense with numerous small vessels (Fig. 3B'). The anterior of the eye is vascularized, albeit sparsely in comparison to the

posterior of the eye. Nasal group papillae sit in relatively large avascular zones surrounded by a sparse vascular network (Fig. 3B’’).

By HH 37 avascular zones in the anterior of the eye have been abolished as well. A dense vascular meshwork composed of many small vessels fills the entirety of the sclera. The same phenotype persists into HH 38 with no noticeable differences arising at this stage (Fig. 3C).

Rather than growing inward towards the cornea from all directions, the vasculature appears to grow only from the posterior of the eye inward toward the cornea and then, once established posteriorly, continues to grow anterodorsally and anteroventrally around the cornea (Fig. 3A, arrows). This results in the formation of avascular zones first around the posterior (temporal) group papillae, then the dorsal and ventral papillae and lastly around the anterior (nasal) papillae. The size of the avascular zone surrounding a specific papilla therefore depends on both the position of the papilla within the eye and on the stage of embryonic development. Furthermore, it is clear that the formation of vasculature does not follow the pattern of formation of the papillae, which is posterior, anterior, dorsal, ventral (see section 1.3).

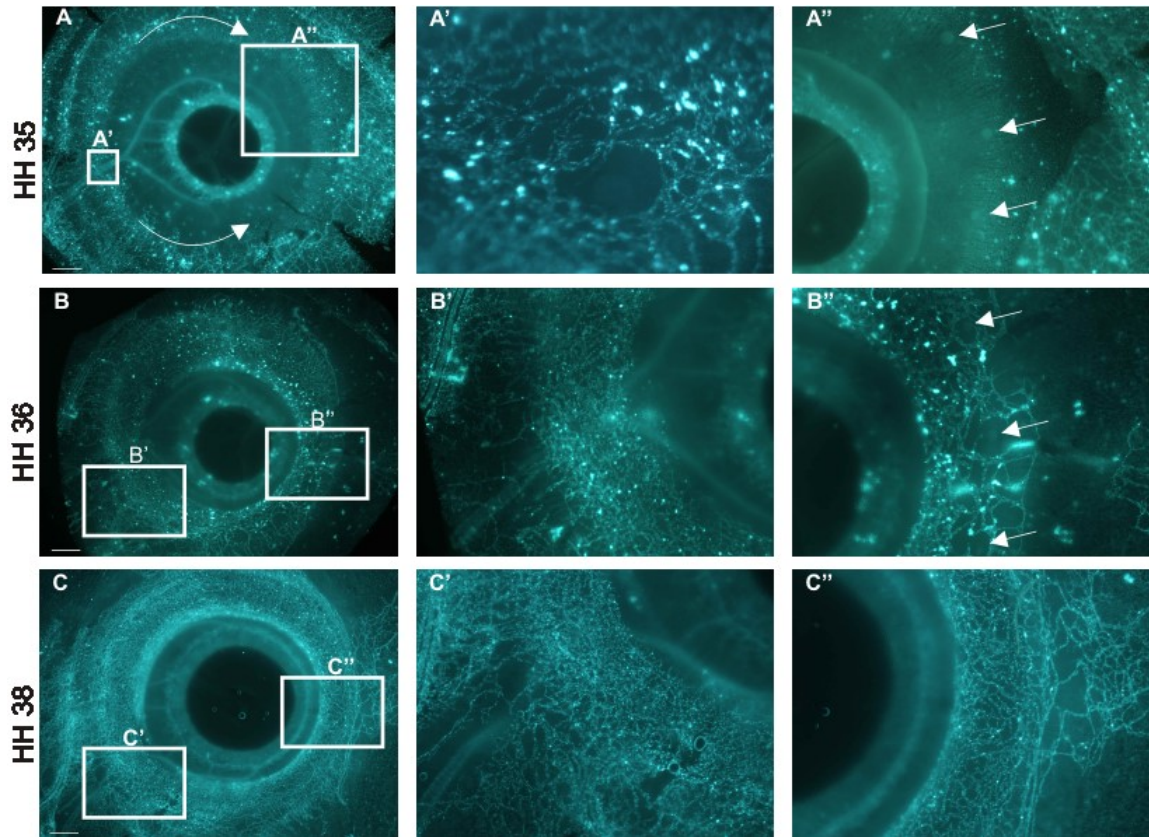


Fig. 3 Vascular growth in the sclera of the chick eye. (A) The vascular network of the sclera at HH 35. A dense vascular meshwork has been established posteriorly, where papillae sit in avascular zones (A'). Arrows show the direction of new vascular growth. Vasculature is absent anteriorly in the region of the papillae (arrows; A''). (B) The vascular network of the sclera at HH 36. The posterior of the eye is well vascularized and avascular zones are no longer present (B'). The anterior of the eye is sparsely vascularized and papillae (arrows) sit in large avascular zones (B''). (C) The vascular network of the sclera at HH 38. The sclera is well vascularized posteriorly (C') and anteriorly (C''). Avascular zones are not present. Scale bars are 500 μm .

3.2 Vegfa In Situ Hybridization

Vegf is known to regulate the processes of angiogenesis (Coultas et al., 2005) and osteogenesis (Liu and Olsen, 2014), and thereby links the two processes (Wang et al., 2007). Although the expression pattern of *vegfa* during endochondral ossification of the mouse limb skeleton has been elucidated in great detail (see section 1.4 for a description; Eshkar-Oren et al., 2009), comparative data for intramembranous bones is not available. In order to determine the spatiotemporal expression pattern of *vegfa* during development of an intramembranous bone, I performed whole mount *in situ* hybridization followed by cryosectioning of stained tissues on chick embryos at stages spanning the entirety of scleral ossicle development (Fig. 1). Specific stages chosen were HH 35 (induction); HH 36.5 (condensation); HH 37.5 (osteoid deposition) and HH 38.5 - 39 (mineralization), as they capture the key events in osteogenesis. Each stage will be described separately.

3.2.1 HH 35 – Induction

Strong *vegfa* expression is detected in conjunctival papillae as well as in underlying and adjacent mesenchyme (Fig.4A, B; n=3). Mesenchymal expression is seen directly below each papilla and extends into the interpapillary zone but in many cases does not fill the entire space (Fig. 4A-B). Cryosectioning of the stained tissue confirms expression in the papilla and reveals that expression is restricted to the cells of the conjunctival epithelium and superficial mesenchyme (Fig. 4C). Cells deep in the mesenchyme, where condensations will later form, do not express the gene at this stage. Controls treated with sense probe or without probe are also shown (Fig. 4D-G).

3.2.2 HH 36.5 – Condensation

The expression pattern of *vegfa* at HH 36.5 is similar to that at HH 35, with expression present in the remaining (non-degenerated) papillae and in the mesenchyme underlying and immediately adjacent to these papillae (Fig. 5A; n=4). However, mesenchymal expression has expanded compared to that seen at HH 35 and is now present throughout the mesenchyme, both superficial and deep (Fig. 5B). Often, a single eye at HH 36.5 will contain both completely degenerated papillae in the temporal region of the eye and partially degenerated papillae elsewhere. In these cases, expression of *vegfa* can be seen in partially degenerated papillae and in the mesenchyme underlying and adjacent to those papillae, whereas expression is decreased or lost in mesenchyme of the temporal region of the eye, where papilla degeneration is complete. Controls treated with sense probe or without probe are unstained (Fig. 5C-F).

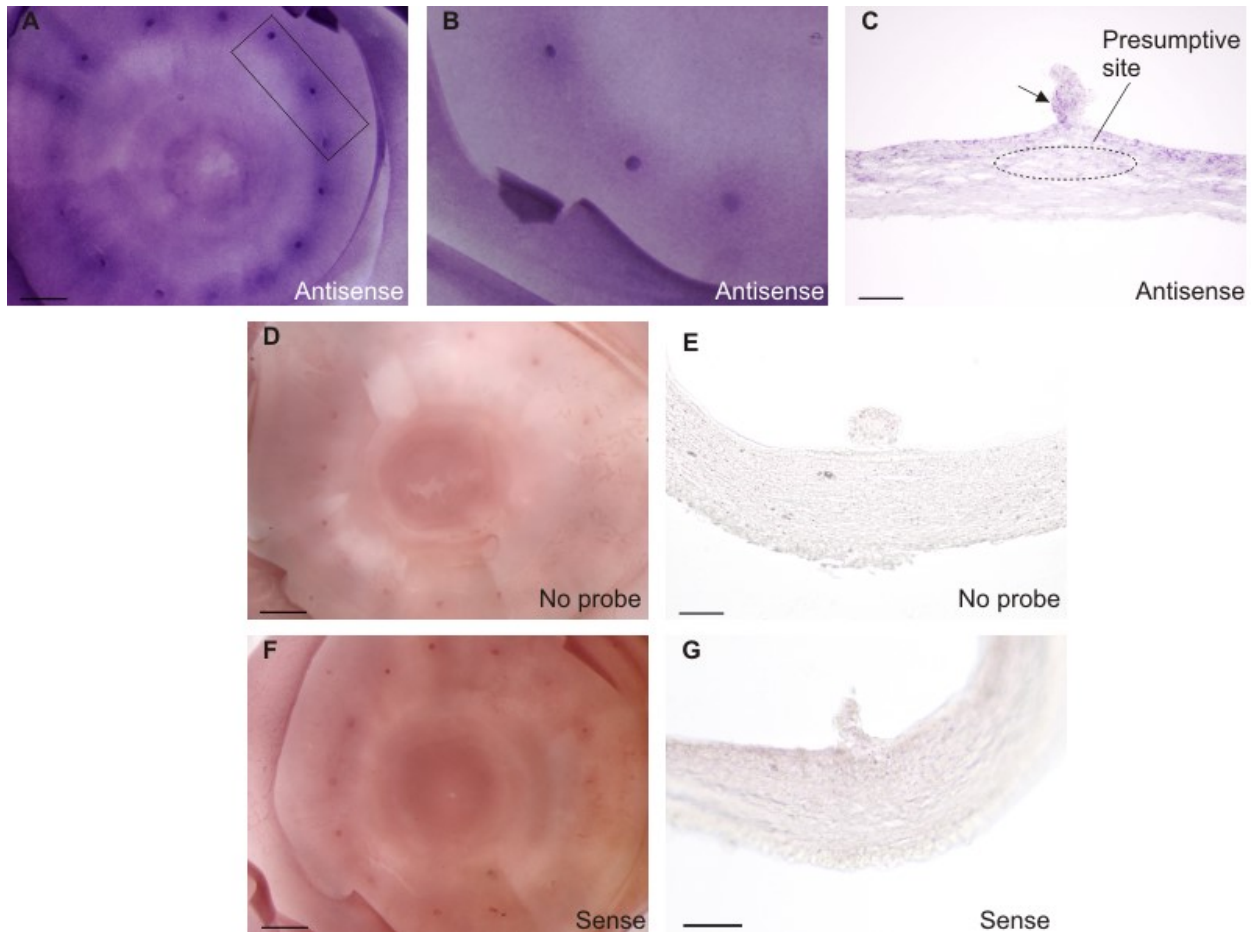


Fig. 4 – *Vegfa* *in situ* hybridization, HH 35 (induction phase). (A) The gene is strongly expressed in the conjunctival papillae as well as in the underlying and immediately adjacent mesenchyme. (B) A close-up of a group of anterior papillae (boxed area in A) showing expression in the underlying and adjacent mesenchyme. (C) Cryosection through an anterior papilla revealing that expression is restricted to the papilla (arrow), conjunctival epithelium and superficial mesenchyme. No expression is seen in the presumptive condensation site (outlined). (D) No probe control showing a lack of *vegfa* expression. (E) No probe control, cryosectioned. (F) Sense probe control showing a lack of *vegfa* expression. (G) Sense probe control, cryosectioned. Scale bars: 500 μm in A, D, F; 50 μm in C, E, G.

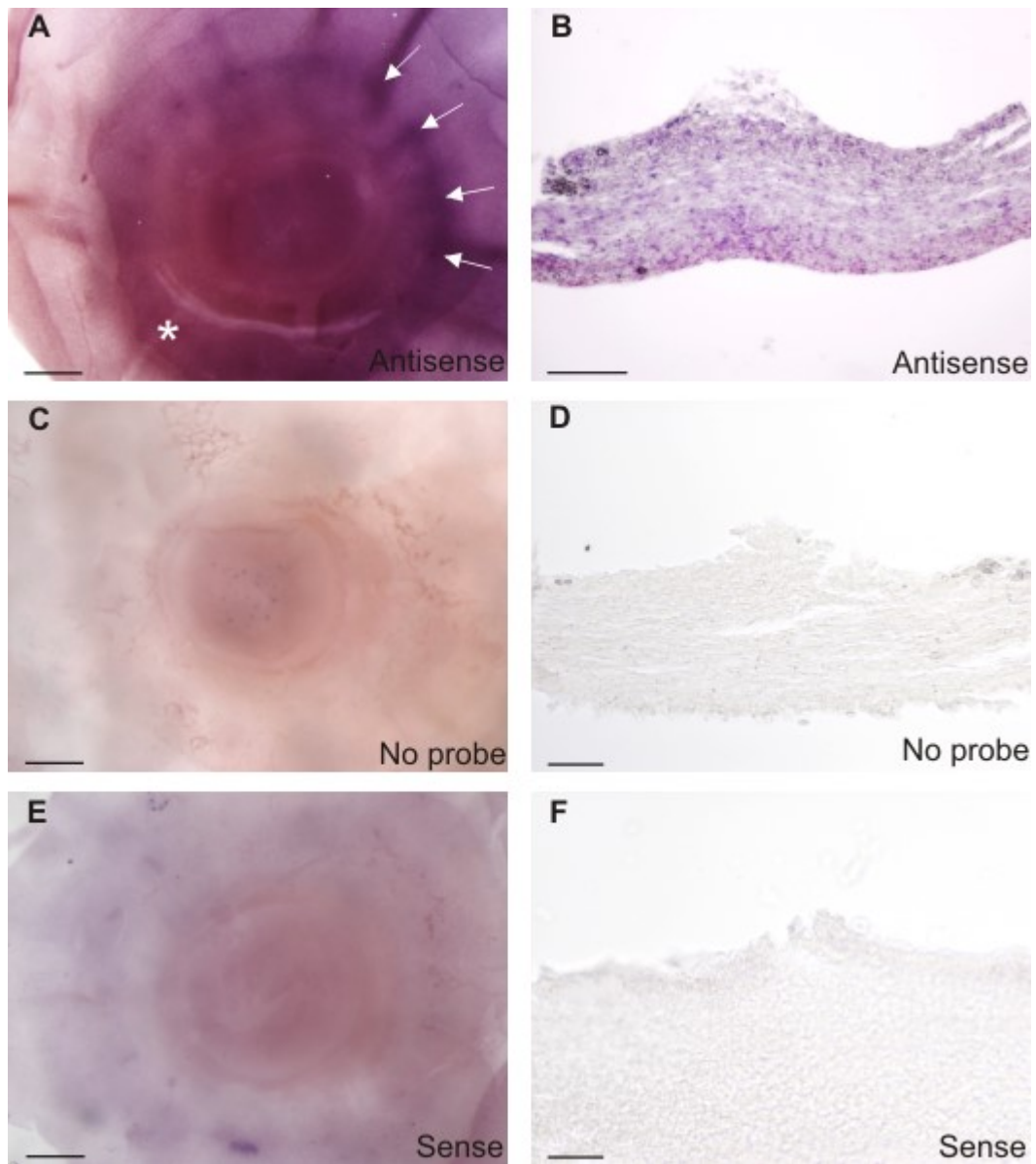


Fig. 5 – *Vegfa* *in situ* hybridization, HH 36.5 (condensation phase). (A) The gene is strongly expressed in the anterior conjunctival papillae (arrows) as well as in the underlying and adjacent mesenchyme, but is lost from the temporal region where papillae have degenerated (asterisk). (B) Cryosection through an anterior papilla revealing that expression is found throughout the mesenchyme. (C) No probe control showing a lack of *vegfa* expression. (D) No probe control, cryosectioned. (E) Sense probe control showing a lack of *vegfa* expression. (F) Sense probe control, cryosectioned. Scale bars: 500 μm in A, C, E; 50 μm in B, D, F.

3.2.3 HH 37 – Osteoid Deposition

Vegfa is expressed in the epithelium and mesenchyme in the anterior of the eye, but not in the condensations themselves (Fig. 6A, B; n=3). Cryosectioning confirms an absence of expression by condensed cells and reveals expression of the gene in conjunctival epithelium and superficial mesenchyme (Fig. 6B). Sense and no probe controls are unstained (Fig. 6C-F).

3.2.4 HH 38.5 – Mineralization

The expression of *vegfa* appeared to be completely turned off by HH 38.5. I was unable to detect expression in any region of the eye, including condensations and surrounding mesenchyme (Fig. 7A, B; n=4). Sense and no probe controls are unstained (Fig. 7C-F).

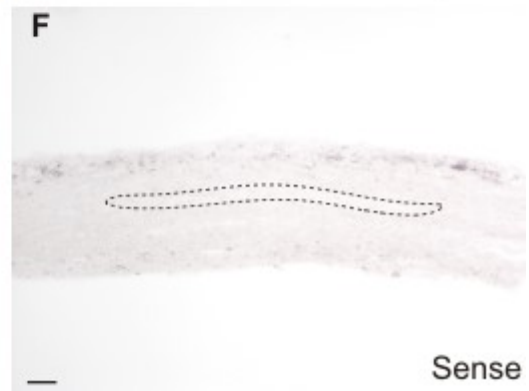
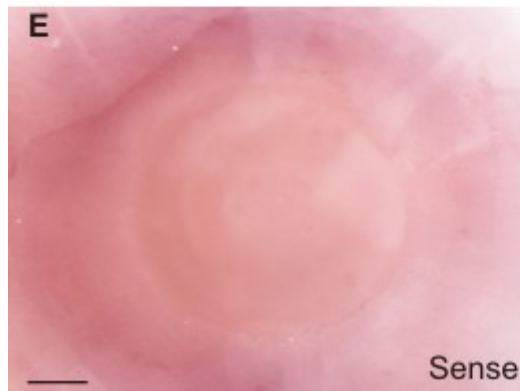
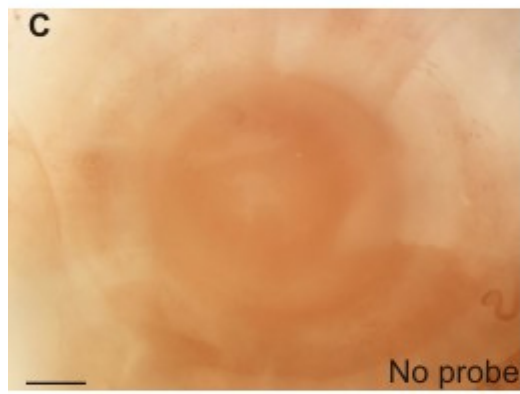
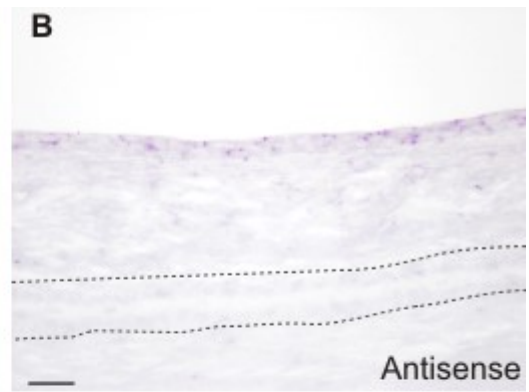
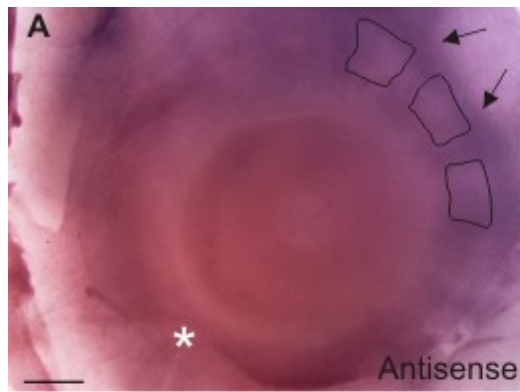


Fig. 6 – *Vegfa* *in situ* hybridization, HH 37.5 (osteoid deposition phase). (A) The gene is not expressed in the temporal region of the eye (asterisk), but expression is detected anteriorly (arrows). Anteriormost condensations are outlined. (B) Cryosection of an anterior condensation showing that expression is restricted to the conjunctival epithelium and superficial mesenchyme. Osteoblasts of the condensations (dashed outline) do not express the gene. (C) No probe control showing a lack of *vegfa* expression. (D) No probe control, cryosectioned. (E) Sense probe control showing a lack of *vegfa* expression. (F) Sense probe control, cryosectioned. Scale bars: 500 μm in A, C, E; 50 μm in B, D, F.

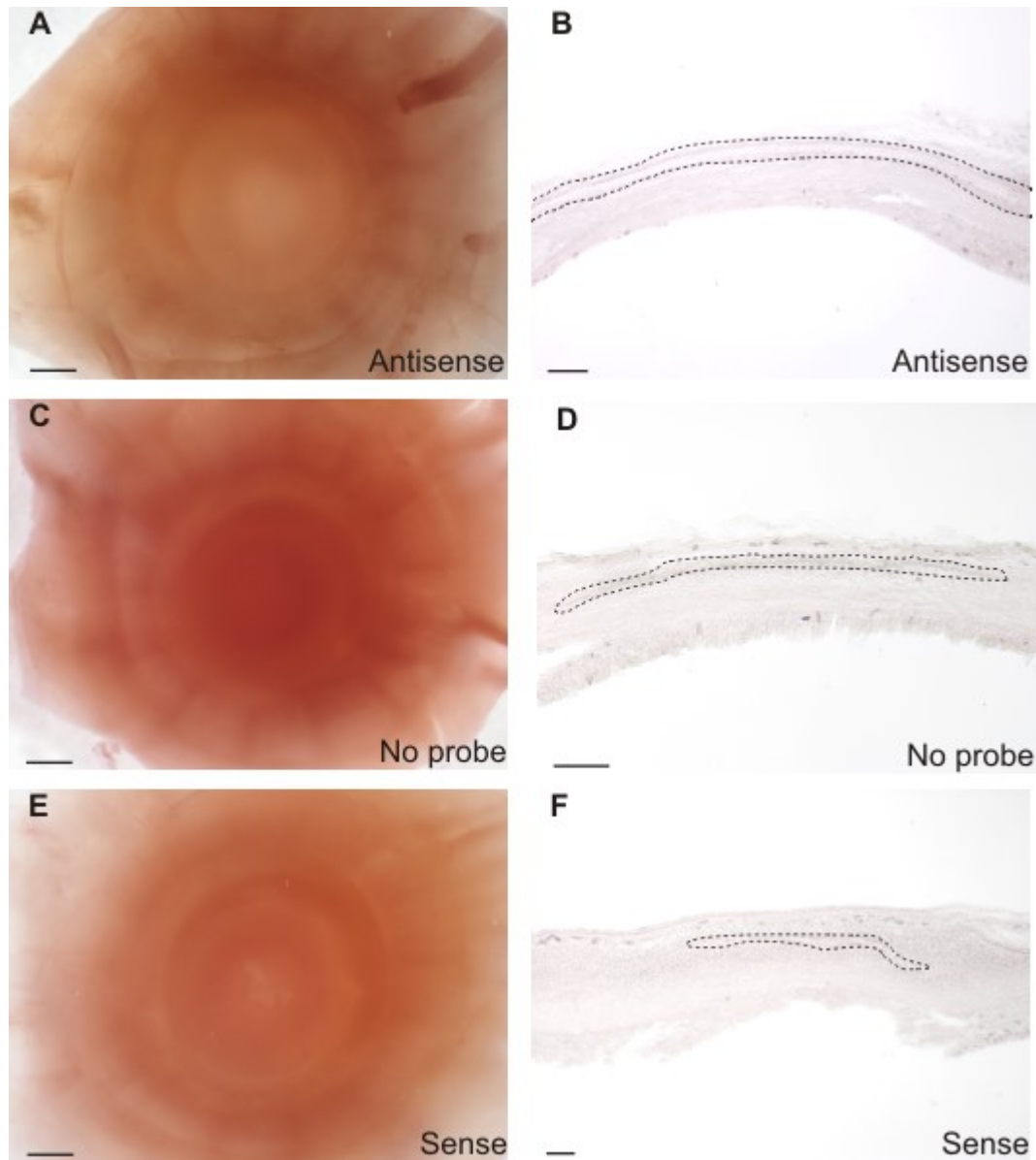


Fig. 7 – *Vegfa* *in situ* hybridization, HH 38.5 (mineralization phase). (A) The gene is not expressed in any region of the eye. (B) Cryosection of an anterior condensation (dashed outline) confirming that the gene is not expressed. (C) No probe control showing a lack of *vegfa* expression. (D) No probe control, cryosectioned. (E) Sense probe control showing a lack of *vegfa* expression. (F) Sense probe control, cryosectioned. Scale bars: 500 μm in A, C, E; 50 μm in B, D, F.

3.2.5 – Summary of In Situ Results

Overall, a clear pattern of expression emerges from the above data. *Vegfa* expression is high at HH 35 in papillae, underlying mesenchyme, and adjacent conjunctival epithelium, and papillae continue to express the gene as they degenerate. Mesenchymal expression is strong during papilla degeneration, but declines once papillae have disappeared. Expression continues to decline until HH 38.5 – 39, when *vegfa* is no longer expressed. Interestingly, induction of underlying condensations, early osteoblast differentiation and establishment of the vascular network of the sclera are all underway at HH 35 and continue throughout HH 36.5, when *vegfa* expression is at its peak. Once condensations and the mature vascular network have become established, expression decreases. Expression at earlier stages of development, as papillae are forming, were not examined.

3.3 Bead Implantation

3.3.1 Effect of sFlt-1 on Scleral Vasculature

In order to determine the role of Vegf in establishment of the scleral vascular network, embryos were implanted with beads containing the Vegf inhibitor sFlt-1 (100 µg/ml; Fig. 8). Each bead was implanted adjacent to a papilla at HH 35 (8.5-9 days of incubation). Growth of the scleral vasculature is ongoing at this time (see section 3.1) and *vegfa* is expressed highly in the epithelium and scleral mesenchyme in and around the papillae (see section 3.2.1). The effect of the bead implant was assessed 1-2 dps at HH 36 (n=11 implanted embryos) or HH 37 (n=22), respectively. Beads soaked in 1x PBS were used as a control (n=3 at 1 dps; n=4 at 2 dps).

If Vegf derived from the papillae and surrounding tissues plays a role in establishment of the scleral vascular network, then blocking it with sFlt-1 should result in an increase in the size of the avascular zone surrounding the bead compared with that of the equivalent papilla in the contralateral eye of the same embryo, which did not receive a bead. Embryos which received beads soaked in 1x PBS should not show a marked difference between the implanted and unimplanted eyes. At 1 dps, the difference in size between the implanted and contralateral unimplanted eye of each embryo was significantly greater for those embryos which received sFlt-1 than those which received 1x PBS (independent 2-sample *t*-test, $t = 2.63$; d.f. = 10; $p = 0.025$; Fig. 8A, B). Additionally, in 45% of sFlt-1 implanted embryos, the avascular zone surrounding the bead was more than 1.5 times the size of the avascular zone surrounding the equivalent papilla in the contralateral eye (Table 1). Such an increase was not observed in any of the 1x PBS controls. Thus, sFlt-1 treatment resulted in an increase in the size of the avascular zone at 1 dps.

Table 1 – Measurement of the area of the avascular zone surrounding the papilla of the bead implanted (right) eye divided by the area of the equivalent papilla of the contralateral (left) eye at 1 day post-surgery in decreasing order of effect. Raw data is in Appendix H.

Experiment number	Treatment	Ratio (Right/Left)
31-8	sFlt-1 (100 µg/ml)	9.39
31-9	sFlt-1 (100 µg/ml)	5.01
25-5	sFlt-1 (100 µg/ml)	2.98
13-6	sFlt-1 (100 µg/ml)	1.76
30-4	sFlt-1 (100 µg/ml)	1.64
30-6	1x PBS	1.41
14-9	sFlt-1 (100 µg/ml)	1.34
29-5	sFlt-1 (100 µg/ml)	1.32
14-7	sFlt-1 (100 µg/ml)	1.25
30-1	sFlt-1 (100 µg/ml)	1.18
31-2	sFlt-1 (100 µg/ml)	1.04
25-2	1x PBS	0.91
30-5	sFlt-1 (100 µg/ml)	0.77
25-1	1x PBS ₅₀	0.76

At 2 dps, embryos had reached HH 37. Previous results have shown that avascular zones are not typically present at this stage (section 3.1); rather, the sclera is filled with a dense meshwork of small vessels. Indeed, no avascular zone could be discerned surrounding sFlt-1-soaked beads in any embryo (n=22; Fig. 8C, D). The same dense meshwork was observed in 1x PBS controls (n=4). Thus, despite the sometimes large effect of the bead on the size of avascular zones at 1 dps, vasculature was able to recover from treatment by 2 dps such that no obvious effect could be discerned.

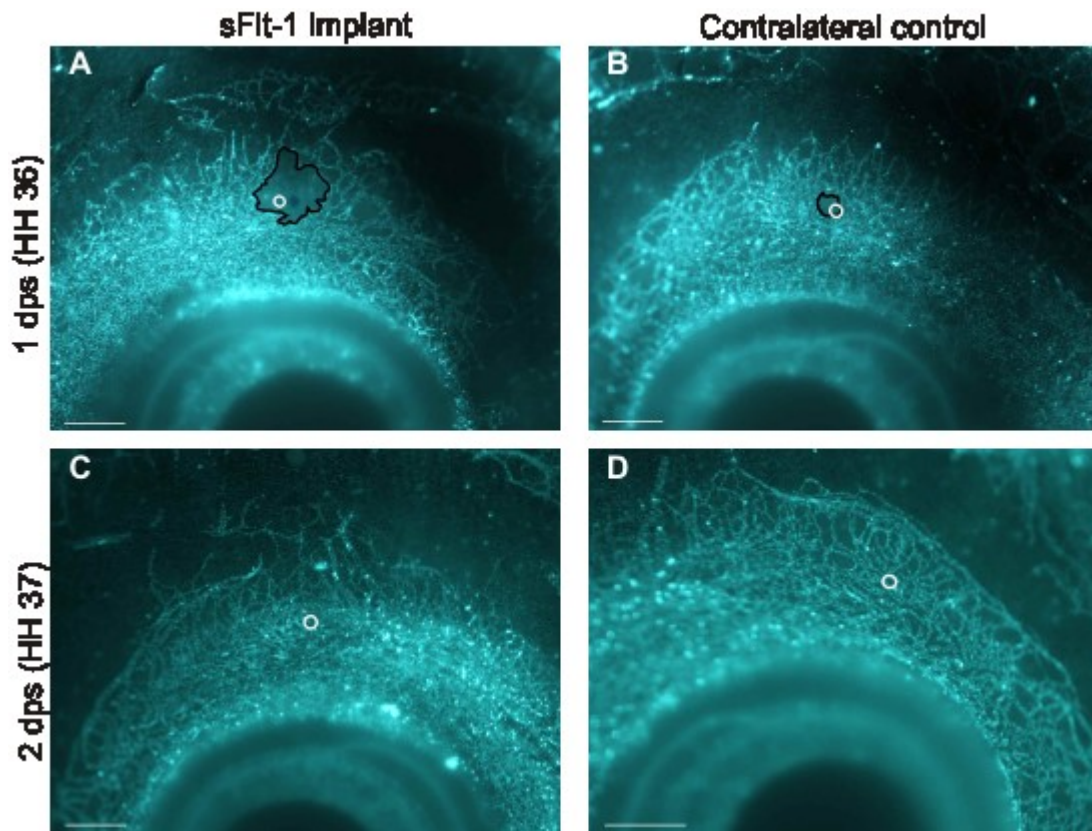


Fig. 8 – Effect of sFlt-1-soaked bead implantation on scleral vasculature. (A-B) Eye implanted with a bead containing 100 $\mu\text{g/ml}$ sFlt-1 at 1 day post-surgery. The avascular zone surrounding the bead (A) is enlarged compared to the contralateral unimplanted eye (B). (C-D) Eye implanted with a bead containing 100 $\mu\text{g/ml}$ sFlt-1 at 2 days post-surgery. An avascular zone is not present in either the implanted (C) or contralateral control eye (D). Avascular zones outlined in black; papillae outlined in white. Scale bars are 500 μm .

3.3.2 Effect of sFlt-1 on Scleral Ossicle Development

In addition to its effects on vasculature, Vegf is thought to play a key role in regulating osteoblast survival (Street and Lenehan, 2009), proliferation (von Schroeder et al., 2003), differentiation (Midy and Plouët, 1994), and synthetic activity (Zelzer et al., 2002) *in vitro*. In order to determine whether Vegf may play a similar role *in vivo*, embryos implanted with a sFlt-1-soaked bead at HH 35 and incubated for 1-2 days (see section 3.3.1) were stained for the presence of alkaline phosphatase (AP). AP is expressed by preosteoblasts and osteoblasts and is considered an early marker for osteoblast differentiation (Franz-Odendaal et al., 2006).


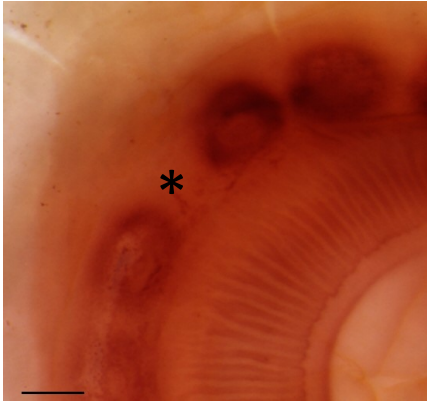
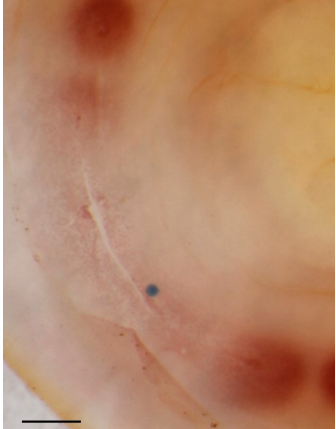
Control (1x PBS)-implanted embryos contained a complete ring of distinct, non-overlapping ossicles at HH 36 and 37 (1 and 2 dps, respectively; Fig. 9A, B). Small deviations were sometimes observed even in unimplanted embryos; such deviations include small regions of ossicle overlap and, rarely, missing ossicles (Franz-Odendaal, 2008). Implanted embryos, on the other hand, often displayed a large deviation from the normal variation. This was true of embryos after both one and two days post-surgery. In these cases, the overall phenotype of each eye can be described as consisting of a number of abnormalities, or mispatterning (Table 2), including: crowding/overlap, gaps between neighboring ossicles, understaining, smearing, missing ossicle or ossicles, formation of an ectopic ossicle or ossicles, and changes in ossicle size and/or shape.


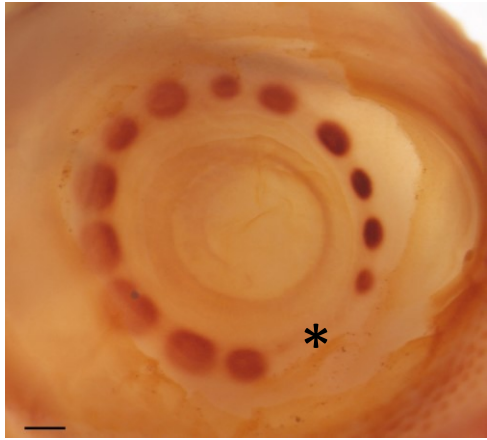

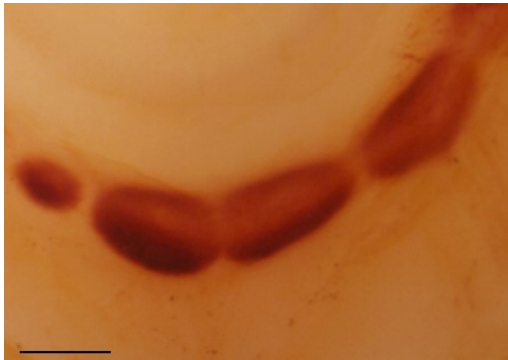
Based on the severity of mispatterning, eyes were classified as one of the following (Fig. 9):

1. Normal – An absence of mispatterning.
2. Mild – Having only one of the above-mentioned mispatterning.

3. Moderate – Having 2-3 of the above-mentioned mispatterings.
4. Severe – Having either greater than 3 mispatterings or a missing/ectopic ossicle.

Table 2 – Common ossicle mispatterning. Scale bars are 500 μ m in each example. See Figures 1 and 9 for examples of normal AP-stained eyes.

Mispatterning	Description	Example
Crowding/overlap	A number of adjacent ossicles remain distinct but are not correctly spaced with respect to one another, thereby resulting in overlap between ossicles	
Gap	Abnormally large space between neighboring ossicles	
Understaining	Ossicles are present but express AP poorly, resulting in a faded appearance	

Mispatterning	Description	Example
Smearing	Neighboring ossicles appear to fuse together such that individual ossicles cannot be discerned	 <p>A micrograph showing a curved row of ossicles. The ossicles are closely spaced and appear to be fused together, making individual boundaries difficult to discern. A small black horizontal scale bar is visible in the bottom-left corner.</p>
Missing ossicle or ossicles	One or more ossicles fail to form	 <p>A micrograph showing a circular arrangement of ossicles. One position in the ring is missing, indicated by a black asterisk (*). A small black horizontal scale bar is visible in the bottom-left corner.</p>
Ectopic ossicle	An additional ossicle forms	 <p>A micrograph showing a curved row of ossicles. An additional, small, dark spot is present between the main row, indicated by a black arrow. A small black horizontal scale bar is visible in the bottom-left corner.</p>
Change in size/shape	An individual ossicle or ossicle of abnormal size and/or shape	 <p>A micrograph showing a curved row of ossicles. One ossicle is significantly larger and more elongated than the others, indicating an abnormal size and shape. A small black horizontal scale bar is visible in the bottom-left corner.</p>

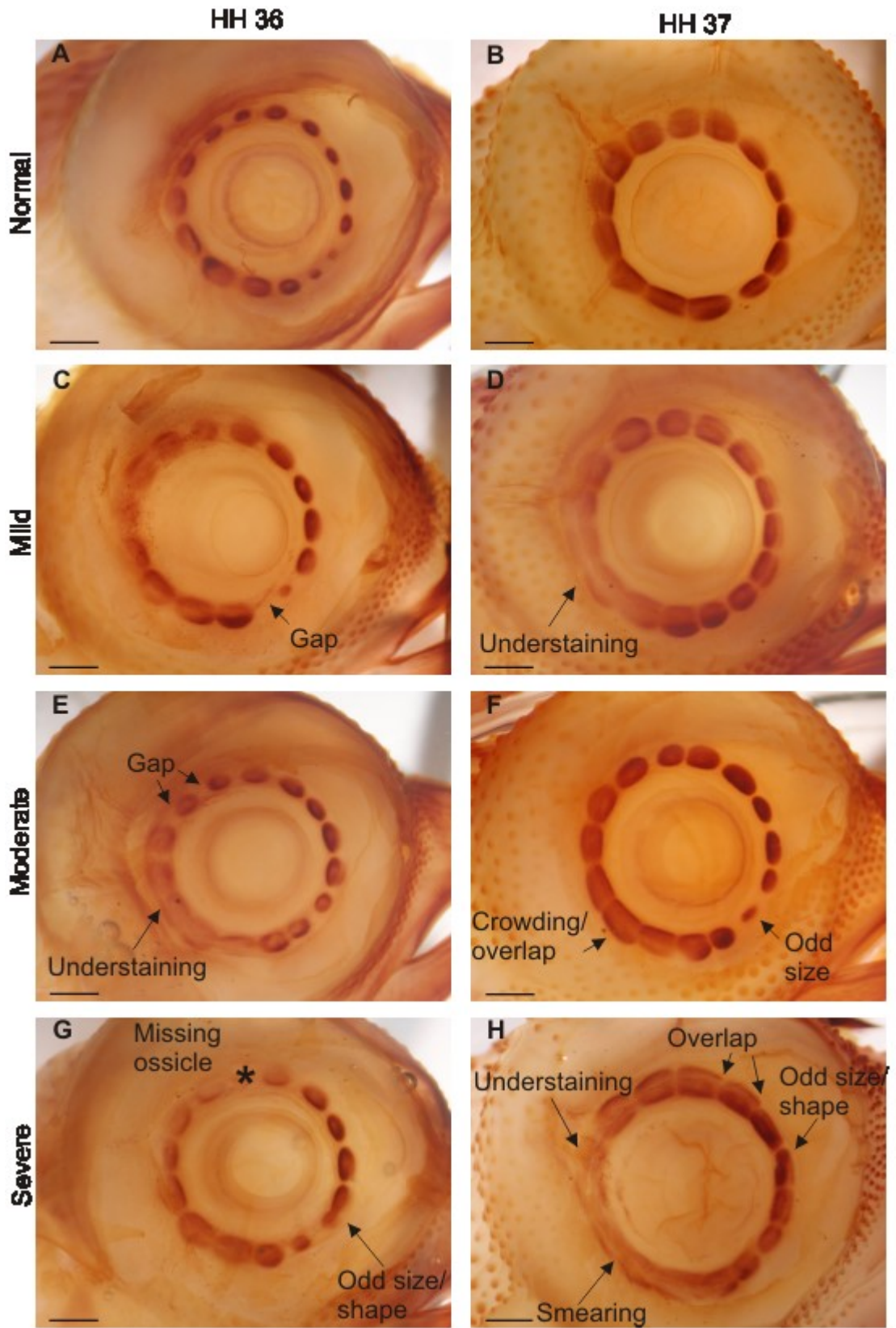


Fig. 9. Classifications of the severity of deviation from the normal pattern of scleral ossicle development following sFlt-1-soaked bead implantation, HH 36 – 37. (A-B) Normal. An absence of mispatterning. (C-D) Mild; one mispatterning. (E-F) Moderate; two to three mispatternings. (G-H) Severe; either an excess of three mispatternings or an ectopic or missing ossicle. Mispatternings are defined in Table 2. Scale bars are 1000 μm .

At 1 dps, 55% of sFlt-1 implanted eyes showed a moderate mispatterning of the ring, compared to only 27% of contralateral unimplanted eyes (Table 3). Furthermore, 27% of implanted eyes showed severe mispatterning, which was never observed in contralateral control eyes. Overall, the severity of ossicle mispatterning in contralateral control eyes tended to be less severe than that of the implanted eye (Table 5; Fig. 10). The process of bead implantation resulted in mild mispatterning in 50% of 1x PBS implanted eyes, with no eye exhibiting either moderate or severe mispatterning.

Table 3 – Relative frequency of the severity of ossicle mispatterning in sFlt-1 versus 1x PBS implanted and contralateral (unimplanted) eyes at 1 day post-surgery.

	Normal	Mild	Moderate	Severe	N
1 dps, sFlt-1, implanted eye	0	18	55	27	11
1 dps, sFlt-1, contralateral eye	27.5	45	27.5	0	11
1 dps, 1x PBS, implanted eye	50	50	0	0	4
1 dps, 1x PBS, contralateral eye	100	0	0	0	4

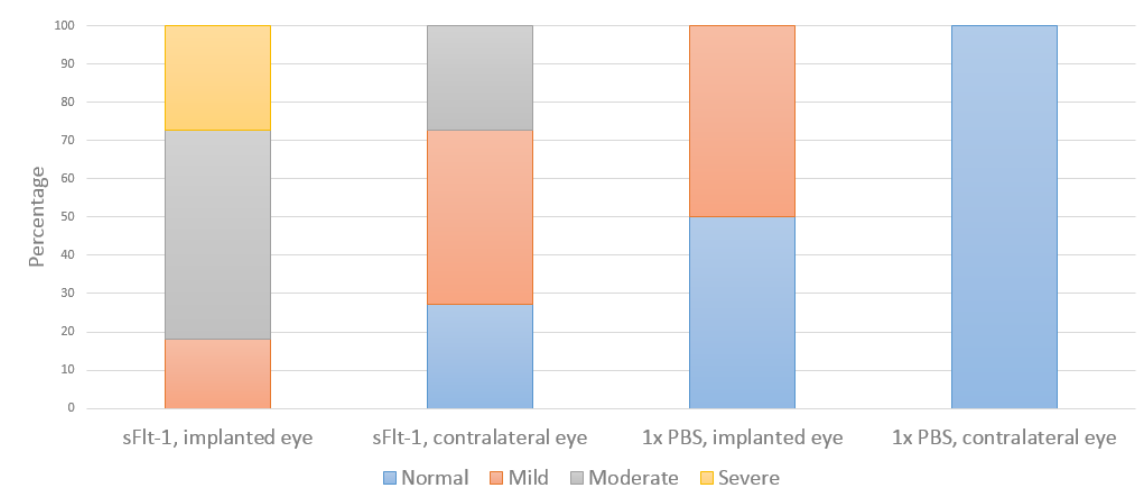


Fig. 10 – Severity of ossicle mispatterning in sFlt-1 versus 1x PBS implanted embryos at 1 day post-surgery. The proportion of embryos falling into each of the four categories of ossicle mispatterning (normal, mild, moderate, severe) are shown for sFlt-1 and 1x PBS implanted eyes, as well as contralateral (unimplanted) eyes. Compared to 1x PBS implants, sFlt-1 implants exhibit a much greater proportion of moderate to severely mispatterned eyes.

Similar ossicle mispatterning were seen at 2 dps. Here, 23% of sFlt-1 implanted eyes showed severe mispatterning of the ring while 32% showed moderate mispatterning (Table 4). Overall, the severity of ossicle mispatterning in contralateral control eyes was similar to that observed for implanted eyes (Table 5; Fig. 11). Here, 27% of contralateral control eyes showed severe mispatterning, and another 27% showed moderate mispatterning. Furthermore, there did not appear to be a clear correlation between the position of bead implantation and the severity of ossicle mispatterning. For instance, implantation adjacent to papilla #12 at HH 35 resulted in severe mispatterning in some embryos and an absence of mispatterning in others (see Table 4 in Appendix I, embryos

24-2 and 24-9, respectively), and the same was true for beads implanted more anteriorly.

The process of bead implantation resulted in mild mispatterning in 25% of 1x PBS implanted and contralateral eyes. Additionally, one of four 1x PBS implanted embryos showed severe mispatterning of the contralateral eye.

Table 4 – Relative frequency of the severity of ossicle mispatterning in sFlt-1 versus 1x PBS implanted and contralateral (unimplanted) eyes at 2 days post-surgery.

	Normal	Mild	Moderate	Severe	N
2 dps, sFlt-1, implanted eye	18	27	32	23	22
2 dps, sFlt-1, contralateral eye	23	23	27	27	22
2 dps, 1x PBS, implanted eye	75	25	0	0	4
2 dps, 1x PBS, contralateral eye	50	25	0	25	4

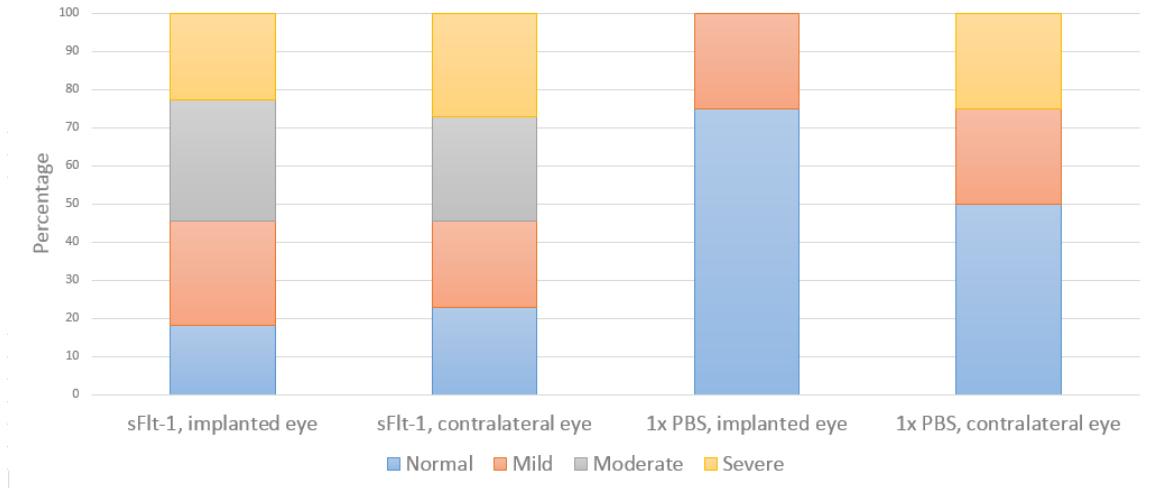


Fig. 11 – Severity of ossicle mispatterning in sFlt-1 versus 1x PBS implanted embryos at 2 days post-surgery. The proportion of embryos falling into each of the four categories of ossicle mispatterning (normal, mild, moderate, severe) are shown for sFlt-1 and 1x PBS implanted eyes, as well as contralateral (unimplanted) eyes. Compared to 1x PBS implants, sFlt-1 implants exhibit a much greater proportion of moderate to severely mispatterned eyes.

The effect of bead implantation is summarized in Figs. 10 and 11, which show the percentages of eyes categorized as normal, mild, moderate or severely mispatterned. These figures reveal a shift in the severity of ossicle mispatterning from primarily normal-mild in 1x PBS implanted embryos to primarily moderate-severe in sFlt-1 implanted embryos at both 1 and 2 dps. The proportion of eyes exhibiting a severe phenotype was also increased in sFlt-1 compared to 1x PBS implants. In addition, it can be seen that at 1 dps, the contralateral eyes of sFlt-1 implants were more severely affected than 1x PBS implanted eyes, but were less severely affected than sFlt-1 implanted eyes.

Interestingly, by 2 dps it appears as though there is little difference in severity between sFlt-1 implanted and contralateral eyes.

These results can be illustrated quantitatively by assigning a numerical value to each category (normal = 0, mild = 1, moderate = 2, severe = 3), summing the values of each group, and taking the average (Table 5). Doing so provides a measure of the severity of mispatterning which ranges from zero to three. This reveals a number of interesting trends. Firstly, sFlt-1 implanted eyes at 1 dps were affected more severely than those at 2 dps (severity = 2.09 and 1.59, respectively), suggesting that ossicles may have been able to recover from treatment. Secondly, contralateral control eyes of sFlt-1 implanted embryos at 1 dps were less severely affected than those at 2 dps (severity = 1 and 1.59, respectively), suggesting that the effect on the contralateral eye was somehow delayed. In fact, there was no difference in the severity of sFlt-1 implanted and contralateral eyes at 2 dps, and both were affected more severely than contralateral eyes at 1 dps (severity = 1.59 and 1, respectively). Thirdly, 1x PBS implanted controls were the least severely affected, as expected, with severity ranging from 0-1. However, that severity was sometimes greater than zero suggests that implantation itself may have had a small effect on ossicle development.

Table 5 – Average severity of ossicle mispatterning in sFlt-1 and 1x PBS implanted embryos at 1-2 days post-surgery. Each of the four categories of ossicle mispatterning (normal, mild, moderate, severe) was assigned a numerical value from 0-3 and an average value was calculated for each group of eyes.

	Average Severity ± Standard Deviation
sFlt-1, implanted eye, 1 dps	2.09 ± 0.70
sFlt-1, contralateral eye, 1 dps	1.00 ± 0.77
1x PBS, implanted eye, 1 dps	0.50 ± 0.58
1x PBS, contralateral eye, 1 dps	0.00 ± 0.00
sFlt-1, implanted eye, 2 dps	1.59 ± 1.05
sFlt-1, contralateral eye, 2 dps	1.59 ± 1.14
1x PBS, implanted eye, 2 dps	0.25 ± 0.50
1x PBS, contralateral eye, 2 dps	1.00 ± 1.41

Chapter 4.0: Discussion

4.1 Conjunctival Papillae and Surrounding Tissues Regulate Growth of Scleral

Vasculature

Through the work of a number of researchers, conjunctival papillae have gradually emerged as key players in scleral ossicle development. Early descriptions of papilla formation were undertaken by Nussbaum (1901) and Dabelow (1927) and were further updated in the 1940's by P.D.F Murray (Murray, 1941, 1943). Through his thorough histological analysis, Murray recognized the close relationship between the papillae and the underlying scleral ossicles, though he was unable to explain the nature of the relationship. Almost 20 years later, Coulombre et al. (1962) provided the first concrete evidence that papillae are required for the formation of ossicles. The results of his studies were two-fold. First, he found that slowing the growth rate of the eye results in a reduction in the number of papillae and, consequently, in the number of ossicles. Secondly, he found that manual removal of a papilla results in the failure of the underlying ossicle to form. Our lab has found that if a papilla is removed without damage to the underlying basement membrane or mesenchyme, the papilla regenerates and properly induces formation of the underlying ossicle (Jourdeuil and Franz-Odenaal, unpublished results). Regardless of the outcome of papilla removal, Murray's conclusion that each papilla is required for the formation of the underlying ossicle remains a valid one (Murray, 1941, 1943).

Hall investigated the papilla-ossicle relationship further by showing that mandibular epithelium can induce scleral mesenchyme to form ossicles, that conjunctival epithelium can induce mandibular mesenchyme to form bony rods (Hall, 1981), and that

this epithelial-mesenchymal interaction occurs via a diffusible signal produced by the epithelium (Pinto and Hall, 1991). Towards identifying this signal or signals, Franz-Odenaal (2008) and Duench and Franz-Odenaal (2012) have found that papillae express *sonic hedgehog (shh)*, *indian hedgehog (ihh)* and *bone morphogenetic protein 2 (bmp-2)* whereas the HH receptor *patched-1 (ptc-1)* is expressed in the papillae and the surrounding mesenchyme (Franz-Odenaal, 2008; Duench and Franz-Odenaal, 2012). Furthermore, inhibition of Shh/Ihh via implantation of a cyclopamine-soaked bead or inhibition of Bmp-2 via implantation of a Noggin-soaked bead at HH 35, when ossicle induction is taking place, has been shown to result in the failure of the underlying ossicle to form (Franz-Odenaal, 2008; Duench and Franz-Odenaal, 2012). These results suggest that Shh/Ihh and Bmp-2 produced by the papillae play a key role in ossicle development. Thus, 110 years after the original description of papilla formation by Nussbaum, we are just beginning to unravel the mysteries of the papilla-ossicle relationship at the molecular level. In this thesis I add one more tissue type to this mystery: the role of the vasculature.

Previous studies from our lab provide, to my knowledge, the first description of scleral vascular growth specifically in relation to the conjunctival papillae and scleral ossicles (Jourdeuil and Franz-Odenaal, 2012). In that study, a combination of camera lucida drawings, erythrocyte autofluorescence and histology were used to map the growth of scleral vasculature from the time of papilla formation (HH 30) through ossicle induction and condensation initiation (HH 36.5). These techniques revealed that the scleral vasculature begins to form *de novo* at HH 34. At this stage, the sclera is filled with a meshwork of open-ended vessels. The vascular network of the eye continues to expand

and avascular zones are present in the mesenchyme underlying and surrounding the conjunctival papillae at HH 36.5 (Jourdeuil and Franz-Odenaal, 2012). I have used a different technique with higher resolution to both confirm and extend the results of this study. Specifically, I found that, although papillae begin to form as early as HH 30, a distinct vascular network is not present in the scleral mesenchyme until HH 35, and at this time is present only in the posterior of the eye. These blood vessels do not fill the entirety of the posterior sclera, but instead form avascular zones underlying the papillae of the temporal region (Fig. 3A'). Such avascular zones have been noted during the development of other skeletal tissues, such as the cartilages of the mouse limb (Eshkar-Oren et al., 2009) and the intramembranous chick frontal bone (Thompson et al., 1989). Avascular zones are further discussed in section 4.2.

In order to determine if *vegfa* plays a role in coordinating the development of the scleral ossicles with that of the scleral vasculature, I performed *in situ* hybridization to detect expression of the gene during key stages of ossicle development (HH 35 – 39). Interestingly, my results show that the spatiotemporal expression pattern of *vegfa* in the chick eye correlates well with the timing of formation and obliteration of avascular zones in the scleral mesenchyme (see sections 3.1 and 3.2). Posteriorly, *vegfa* is expressed at HH 35, when avascular zones are present and blood vessel growth is ongoing, and has decreased by HH 36.5, when avascular zones have been obliterated and vascular growth has slowed or stopped. Anteriorly, *vegfa* is also expressed at HH 35, when this region of the eye is completely avascular, and extends into HH 36.5, when avascular zones are present. Expression even extends into HH 37, when avascular zones have been obliterated but some vascular remodeling is presumably occurring. Thus, *vegfa* is highly

expressed during blood vessel growth and is downregulated once the vascular network has been established. Papillae express the gene highly throughout these stages (section 3.2), thereby making them an important source of secreted Vegf during growth of scleral vasculature.

Furthermore, I have shown that blocking Vegf via implantation of a bead soaked in sFlt-1 results in a significant expansion in the size of the avascular zone at the site of implantation. It should be noted that sFlt-1 inhibits the function of Vegf protein, whereas *in situ* hybridization detects the presence of *vegfa* messenger RNA. Although *vegfa* is expressed primarily by the papillae and superficial mesenchymal tissues, Vegf may act at some distance from its source (Robinson and Stringer, 2001). Thus, sFlt-1 does not necessarily affect the same tissues which express *vegfa*. Furthermore, although numerous studies utilize Affi-gel blue beads, the rate of diffusion of protein from these beads has not been adequately described. For instance, does the protein diffuse all at once as a single large dose, or are small quantities released over a prolonged period of time? Knowledge of the diffusion rate of sFlt-1 from the bead would clearly be useful in interpreting experimental results. Although the diffusion rate of sFlt-1 is unknown, experiments in which beads soaked in Spotlister highlighter ink were implanted into the chick sclera suggest that the solution leaves the bead within the first few hours of implantation (unpublished observation). The effect of the bead is closely related to the timing of implantation: when implanted too long before or too long after the establishment of avascular zones, the bead had little to no effect. However, when implanted just prior to avascular zone establishment, an increase in avascular zone size of more than double the area of the equivalent papilla in the contralateral eye of the same

embryo was observed at 1 dps (n = 3). The greatest effect was an increase in area of over nine times. This result further supports the conclusion that Vegf regulates scleral angiogenesis, and highlights the key importance of timing in this process. Since this effect is no longer apparent at 2 dps, it seems that sFlt-1 is able to delay blood vessel growth but does not stop it indefinitely. These results demonstrate that Vegf produced by the papillae and surrounding tissues (conjunctival epithelium, superficial scleral mesenchyme) plays a key role in regulating the growth of scleral vasculature.

The formation of an avascular zone requires not only angiogenic factors, such as Vegf, but antiangiogenic factors as well (Meadows et al., 2012). Oddly, tissues destined to remain avascular (such as the cornea) have been shown to produce a number of both angiogenic (Vegf, Fgf-2, Pdgf-2) and antiangiogenic (sFlt-1, Semaphorin-3a, Netrin-4) proteins (Kwiatkowski et al., 2013). Clearly, then, angiogenesis relies not only on the presence or absence of angiogenic/antiangiogenic factors, but on the balance between the two. This draws parallels with condensation formation during tooth morphogenesis, which requires both attractive and repulsive signals to promote formation of high cell density (Mammoto et al., 2012). To date, the expression of antiangiogenic proteins during scleral ossicle development has not been explored, with the exception of members of the thrombospondin gene family. Thrombospondins are a group of closely related extracellular matrix molecules thought to play key roles in regulating angiogenesis (Adams and Lawler, 2011). Thrombospondin-4, but not thrombospondin-2, is expressed by the cells of scleral ossicle condensations at HH 36 (Tucker et al., 1995). Although thrombospondin-2 is well known for its antiangiogenic properties, the function of thrombospondin-4 is largely unknown, and there is no evidence to support an

antiangiogenic function for this protein (Bornstein, 2009). However, given its timing and location of expression, and its close structural relationship with antiangiogenic members of the thrombospondin gene family, thrombospondin-4 remains a potential key mediator of avascular zone formation during scleral ossicle development.

4.2 Expansion of Avascular Zones is Not Sufficient to Promote Osteogenesis

Avascular zones do not persist indefinitely but rather gradually decrease in size until they are eventually abolished. In the posterior (temporal) region of the eye, avascular zones are present at HH 35, a full 36 hours before condensations are apparent histologically (Jabalee et al., 2013), and have been abolished by HH 36.5, once condensations have initiated. The timing of these events suggests that avascularity may be a requirement for the initial stages of osteogenesis, such as condensation induction and formation. Indeed, Yin and Pacifici (2001) have shown that when the formation of the avascular zone preceding the formation of the digit 2 cartilage of the chick limb is abolished by implanting a bead soaked in Vegf, the cartilage element fails to form (Yin and Pacifici, 2001), suggesting that avascular zones are required for this process.

In order to determine if avascular zone size plays a role in early scleral ossicle development, I implanted beads soaked in the anti-angiogenic protein sFlt-1, thereby causing an expansion of the avascular zone at 1 dps. My results do not suggest a correlation between the increase in the size of the avascular zone and the severity of ossicle mispatterning. For instance, the two embryos which show the greatest increase in avascular zone size at 1 dps (embryos 31-8 and 31-9; Appendix H) show only moderate and mild mispatterning of ossicles, respectively, and the ossicle directly below the bead

does not appear significantly altered in size or shape in either embryo, as evidenced by alkaline phosphatase staining. Furthermore, embryos which show little to no expansion of the avascular zone at 1 dps can show a severe phenotype (e.g., embryo 31-2; Appendix H, I). However, sample number here is low. Additionally, the unimplanted contralateral eyes of sFlt-1 implanted embryos often exhibit an abnormal ossicle phenotype even when vasculature appears to be unaffected. These observations suggest that increasing avascular zone size does not have a significant effect on scleral ossicles. This may be because avascularity itself is not sufficient to promote osteogenesis; for instance, a combination of avascularity and some inductive signal (such as *Ihh/Shh* or *Bmp-2*) may be required for osteoblast differentiation or condensation formation to occur. If this were true, expansion of an avascular zone would not affect scleral ossicle development because the inductive signal remains unchanged. Interestingly, just such an effect was documented by Salim et al. (2004). In their study, the authors showed that calvaria-derived osteoblasts exposed to anoxic conditions (extracellular oxygen concentration of <0.02%) exhibit a decrease in expression of the key osteogenic factor *runx2*. *Runx2* expression could be rescued in anoxic cultures by addition of exogenous *Bmp-2* (Salim et al., 2004). Furthermore, *Bmp-2* and *Vegf* have been shown to interact to regulate bone vascularization and osteoblast differentiation during endochondral ossification (Yang et al., 2013). Interestingly, *bmp-2* is strongly expressed in conjunctival papillae at HH 34.5, coincident with the beginning of ossicle induction, and continues until early HH 36 when posterior avascular zones are obliterated (Duench and Franz-Odenaal, 2012), and therefore its expression partially overlaps with that of *vegfa* both spatially and temporally.

Notably, the converse experiment, in which an avascular zone is obliterated prematurely, has not been performed for an intramembranous bone.

Why do avascular zones form prior to osteogenesis at all? Although there is no definitive answer to this question, recent experiments suggest two potential explanations: hypoxia and endothelial cell inhibition of osteoblast differentiation. These possibilities are discussed in turn below.

Avascular zones surrounding the condensations of mouse digits are low in oxygen, or hypoxic (Amarilio et al., 2007). During chondrogenesis, hypoxia acts to upregulate the expression of the key chondrogenic gene *sox9* in chondrocytes, thereby promoting cartilage formation (Amarilio et al., 2007). This is due to a direct interaction between hypoxia inducible transcription factor 1 (Hif-1) and the *sox9* promoter (Amarilio et al., 2007). Likewise, osteoblasts lining the mandible (an intramembranous bone) have been shown to express Hif proteins as well (De Spiegelaere et al., 2010). Despite this, the role of Hifs during intramembranous ossification have not been explored and little to no evidence exists to suggest that hypoxia is a positive regulator of osteogenesis as it appears to be for chondrogenesis. In fact, Utting et al. (2006) have shown that cultures of calvaria-derived osteoblasts harvested from neonatal rats exhibit a decrease in proliferation and expression of the key osteogenic genes *alkaline phosphatase* and *osteocalcin* when grown under hypoxic conditions (Utting et al., 2006), and numerous authors agree that hypoxia inhibits osteoblast differentiation (Park et al., 2002; Salim et al., 2004). It should be noted that these studies utilize differentiated osteoblasts, and similar studies using preosteoblasts or undifferentiated cells with skeletogenic potential

are therefore required. Thus, the role of hypoxia during intramembranous ossification remains poorly studied at this time, particularly *in vivo*.

A second possibility is that endothelial cells may inhibit osteoblast differentiation via a mechanism that involves short-range paracrine signaling and/or direct cell-to-cell contact. Interestingly, Meury et al. (2006) have found that human bone marrow stromal cells differentiate into osteoblasts when grown in osteogenic medium, but not in the presence of human umbilical vein endothelial cells (Meury et al., 2006). On the other hand, similar experiments have shown that endothelial cells have a positive effect on the survival and differentiation of human primary osteoblasts (Simunovic et al., 2013), suggesting that the effects of endothelial cells depend upon the precise cell type with which they are in contact. To further this point, *in vivo* studies of murine long bones by Kusumbe et al. (2014) suggest the existence of a distinct subtype of endothelial cell, termed a Type H endothelial cell, which preferentially associates with osteoprogenitor cells and regulates their differentiation into osteoblasts (Kusumbe et al., 2014) via a mechanism involving the Bmp antagonist Noggin (Ramasamy et al., 2014). As with hypoxia, the role of endothelial cell-osteoblast interactions during intramembranous ossification has been poorly studied, and *in vivo* studies of this phenomenon are lacking.

4.3 Vegf Regulates the Early Stages of Intramembranous Ossification *In Vivo*

In addition to its role in regulating angiogenesis, Vegf is thought to play a role in promoting osteoblast differentiation and, ultimately, bone formation. Evidence for this comes mainly from *in vitro* studies of osteoblasts or osteoblast precursors exposed to exogenous Vegf. Calvaria-derived preosteoblasts express *vegfa* and its receptors (*vegfr-1*,

vegfr-2, and *nrip1*; Deckers et al., 2000). The expression of *vegfa* and *vegfr* is low during early differentiation, but increases as mineralized bone nodules begin to form (Deckers et al., 2000). Furthermore, the addition of exogenous Vegf to preosteoblast cultures results in an increase in *alkaline phosphatase* expression (Midy and Plouët, 1994) and bone nodule formation (Deckers et al., 2000), suggesting that it is a positive regulator of osteogenesis.

The expression pattern of *vegfa in vivo* is more complex. During endochondral ossification, *vegfa* is expressed diffusely throughout the mesenchyme at the time of condensation formation, becomes restricted to the cartilage element at early stages of development, and becomes further restricted to the hypertrophic zone of the cartilage at the onset of endochondral ossification (Eshkar-Oren et al., 2009). During scleral ossicle development, *vegfa* is expressed diffusely throughout the scleral mesenchyme transiently at HH 36.5, and this is similar to the diffuse expression observed throughout the limb bud mesenchyme in early limb development (Eshkar-Oren et al., 2009). Unlike during endochondral ossification, however, *vegfa* expression does not become localized to the skeletal cells as development proceeds. Indeed, expression was not detected in ossicle condensations at HH 37.5 and, unlike in osteoblast cultures, expression was not found to increase at the time of mineralization of chick scleral ossicles (HH 38.5-39). It should be noted that it is possible that *vegfa* is expressed at HH 38.5-39 in ossicle condensations but is not detected by whole mount *in situ* hybridization. It may be that the expression of *vegfa* is too low to be detected by *in situ* hybridization at this stage, or may be a result of the advanced age of the embryos. This technique becomes more difficult as chicks grow. As tissues age, their extracellular matrices become more dense, making it more difficult

for reagents to penetrate the deeper tissues. To mitigate this, I attempted the protocol with different concentrations of Proteinase K, which serves to digest the tissue, prior to treatment with probe. Regardless, I was unable to detect any *vegfa* expression at this stage. Use of a more sensitive technique, such as PCR, or sectioning of tissue prior to *in situ* would help to confirm the absence of the gene at late stages. Overall, differences in *vegfa* expression are observed during the development of endochondral and intramembranous bones. Regardless, the expression pattern of *vegfa* during scleral ossicle development suggests a potential role for Vegf in the early stages of osteogenesis.

Zelzer et al. (2002) used genetically engineered mice in order to study the role of Vegf during intramembranous bone development *in vivo*. These mice express only the 120 amino acid isoform of Vegf and lack the other five (Zelzer et al., 2002). Interestingly, these mice exhibit undervascularization and undermineralization of the calvariae (Zelzer et al., 2002), suggesting that Vegf signaling is required for their formation. Likewise, localized knockdown of Vegf signaling in the HH 35 chick eye results in a number of ossicle abnormalities 1-2 dps. Of these, changes in condensation size and shape, as well as decrease or loss of alkaline phosphatase are the most common. Interestingly, bead implantation relatively early in ossicle formation tends to correlate well with understaining and ossicle loss, whereas implantation relatively late in ossicle formation tends to correlate well with changes in ossicle size and shape (e.g., embryo 29-5 for early and embryo 31-2 for late; Appendix I). This result suggests that the role of Vegf is dependent upon the stage of bone formation. That early implantation tends to result in understaining or ossicle loss suggests that Vegf is required for early osteoblast differentiation. Implantation of sFlt-1-soaked beads followed by analysis of the

expression of other key osteogenic factors, such as *runx2* and *osterix*, will help to confirm this. Alternatively, *Vegf* may be necessary for cell survival, as is true of chondrocytes (Zelzer et al., 2004). Analysis of apoptosis in sFlt-1 implanted embryos will be necessary to determine if this is the case. That late implantation tends to result in changes in ossicle size and shape suggests that *Vegf* may play a role in regulating condensation boundaries. Analysis of the distribution of key boundary molecules, such as syndecan and tenascin C (Hall and Miyake, 2000), in sFlt-1 implanted embryos will provide insight into this problem.

4.4 Implantation of sFlt-1-Soaked Beads Results in Widespread, Rather Than Local, Effects

The effects of sFlt-1 bead implantation are not localized to the ossicle directly below the bead. Instead, numerous ossicles within the implanted eye and even the ossicles of the contralateral, unimplanted eye are affected. Previous experiments in our lab have shown that loss of an ossicle as a result of *Ihh/Shh* or *Bmp* inhibition prompts the remaining ossicles to compensate by increasing in size to fill the gap left by the missing ossicle (Franz-Odenaal, 2008; Duench and Franz-Odenaal, 2012). Such accommodation leads to a complete sclerotic ring despite the presence of one fewer ossicle. However, the ossicles of the contralateral unimplanted eye of these embryos appeared normal (Franz-Odenaal, 2008; Duench and Franz-Odenaal, 2012) and such compensation was not observed in the present study. One potential explanation for these observations relates to the timing of the experiments of Franz-Odenaal (2008) and Duench and Franz-Odenaal (2012). I analyzed the effects of bead implantation 1-2 dps,

while Franz-Odenaal (2008) and Duench and Franz-Odenaal (2012) analyzed the effects of bead implantation 3-6 dps, allowing more time for recovery from treatment. Thus, early abnormalities that later recover may not have been apparent in those studies; however, some effects are unlikely to recover. Indeed, Yin and Pacifici (2001) have shown that implantation of a Vegf-soaked bead above digit 2 of the chick limb results in obliteration of the underlying cartilage element after 2 days, but embryos were able to fully recover from treatment by 6 dps (Yin and Pacifici, 2001). It would be interesting to determine if ossicles are capable of such recovery after a prolonged period of incubation following sFlt-1 bead implantation. Interestingly, Yin et al. (2002) described quite a different result. These authors implanted beads soaked in the antiangiogenic compound squalamine above the humerus of the chick limb just prior to the onset of chondrogenesis. This treatment resulted in a decrease in humeral length only after 3-4 dps; prior to this, all embryos were normal (Yin et al., 2002). Clearly these types of experiments are extremely time sensitive.

Ossicle mispatterning in contralateral unimplanted eyes of sFlt-1 implanted embryos is not due to membrane dissection or surgery, as 1x PBS controls do not generally show a severely abnormal phenotype. How then are contralateral ossicles affected? Currently there is no satisfactory explanation. One possibility is that sFlt-1 enters the vascular network near the site of implantation and is released from blood vessels at distant sites (i.e. into the scleral mesenchyme of the contralateral eye). Although sFlt-1 is secreted into the blood by endothelial cells under normal conditions (Jung et al., 2012), its uptake from one site and release at a distant site has not been previously described. However, it is interesting to note that the anteriormost ossicles of

the contralateral unimplanted eye, which have not yet been approached by vasculature at the stage of implantation, are rarely affected. Instead, it tends to be the ossicles in the posterior of the eye, which is well vascularized at both the time of implantation and the time of fixation, that show an abnormal phenotype (33% of anterior group ossicles display obvious mispatterning compared to 84% of posterior group ossicles in contralateral eyes of sFlt-1 implanted embryos). Interestingly, the optic nerve from each eye crosses with that of the contralateral eye at the optic chiasm, and the cerebrospinal fluid surrounding these nerves provides a direct path from one eye to the other (Jeffrey, 2001; Killer et al., 2007). Thus, it is conceivable that sFlt-1 could diffuse from the site of implantation in the right eye to the sclera of the left eye by way of the optic chiasm or via another route. Implantation of a bead soaked in sFlt-1 which has been fluorescently tagged would allow diffusion and localization of the protein to be analyzed in real time, thereby providing a means to determine if movement of sFlt-1 into the contralateral eye actually occurs. Unfortunately, no literature regarding vascular connection between the eyes of the chick could be found.

Interestingly, this is not the first time that manipulation of one eye was reported to cause a change in the contralateral side of the head. Recent studies from our lab have shown that removal of the lens from the eye of a 1 day old Mexican tetra increases the expression of *pitx2*, thought to play a key role in regulating craniofacial development, in the forebrain on the opposite side of the head and decreases it in the surgery eye and jaw (Atukorallaya and Franz-Odenaal, unpublished results). These results, both intriguing and perplexing, are worthy of additional study.

4.5 Conclusions

Intramembranous bone development relies heavily on interactions between bone cells and surrounding tissue types. Such interactions occur throughout bone development and are essential in producing a bone of the proper size and shape, in the proper location, and at the proper time during development. This study utilized the scleral ossicles of the chick embryo, a useful but underappreciated developmental system, in order to understand how a specific tissue type, the embryonic vasculature, regulates the development of intramembranous bone.

To begin, the growth of scleral vasculature was examined in relation to the development of the conjunctival papillae and scleral ossicles. These experiments revealed an intimate relationship between vascular growth and bone development. Distinct avascular zones surround the conjunctival papillae at the time of ossicle induction and are later obliterated, concomitant with the end of induction and the degeneration of the papillae themselves. Such coordination hints at a requirement for avascularity in the early stages of bone development, such as induction and condensation. However, just what function avascular zones serve remains unknown.

The expression pattern of *vegfa* suggests that this gene plays a key role in coordinating vasculature and bone development. In the posterior of the eye, *vegfa* is highly expressed at HH 35, when both vascular growth and ossicle induction are taking place, and is downregulated by HH 36.5, when both such events have ended. Interestingly, expression is largely confined to the papillae and surrounding superficial mesenchyme, except for a brief period during which expression is seen throughout the

mesenchyme. Contrary to the results of *in vitro* studies, *vegfa* appears to be downregulated at the time of scleral ossicle mineralization.

Implantation of beads soaked in a Vegf inhibitor, sFlt-1, were used to gain insight into the roles of Vegf in regulating vascular growth within the scleral connective tissue. This treatment resulted in an expansion of the size of the avascular zone in the mesenchyme below the bead at 1 dps, suggesting that Vegf is indeed required for proper patterning of the scleral vasculature. Thus, the conjunctival papillae not only induce scleral ossicle formation but play a key role in regulating scleral vascularization. This is in contrast to chondrogenesis of the limb skeleton, during which skeletal elements themselves are the primary source of Vegf regulating limb vascularization (Eshkar-Oren et al., 2009). That expansion of the avascular zone is no longer apparent by 2 dps suggests the vasculature is able to recover from the treatment.

Finally, the role of Vegf in the development of the scleral ossicles themselves was investigated. Implantation of sFlt-1-soaked beads resulted in a number of ossicle mispatterning at 1 and 2 days post-surgery. Common mispatterning include a decrease in alkaline phosphatase and ossicle loss, indicative of a role for Vegf in osteoblast differentiation. Changes in ossicle size and shape were also common, indicative of a role for Vegf in determining condensation boundaries. Both of these possibilities warrant further investigation, and scleral ossicles provide an excellent model in which to perform such experiments.

In summary, this research has provided much insight into the complex relationship between bone cells and blood vessels during development of intramembranous bones (Table 6). It is my hope that this study will inspire others to

continue to pursue the details of these interactions, and to push our understanding ever further. In a field dominated by cell culture, scleral ossicles provide a fresh *in vivo* system in which to tackle such pursuits.

Table 6 – Summary of developmental events during the formation of scleral ossicles.

Developmental Stage (HH)	Papillae/Condensations	Vasculature	<i>Vegfa</i> expression
30	First papilla (#12) forms over the ciliary artery		
31	Remaining temporal papillae (#10-14) form and nasal papillae (#2-6) begin to form		
32	Nasal group papillae have formed		
33	Dorsal group papillae form		
34	Ventral group papillae form, with the last papilla (#1) forming over the choroid fissure	Vasculogenesis occurs in the sclera (Jourdeuil and Franz-Odenaal, 2012)	
35	Induction	Vasculature network absent anteriorly; vasculature surrounds temporal papillae forming avascular zones	Strong expression in papillae and superficial mesenchyme anteriorly and posteriorly

Developmental Stage (HH)	Papillae/Condensations	Vasculature	<i>Vegfa</i> expression
36	Condensation #12 visible histologically; temporal papillae degenerate	Anterior avascular zones present; posterior avascular zones obliterated	Strong expression throughout mesenchyme anteriorly; decreased posteriorly
37	Condensations well-formed; osteoid deposition underway in all condensations; nasal, dorsal and ventral papillae degenerate	Homogeneous vascular network throughout the sclera; all avascular zones obliterated	Expression in superficial mesenchyme and conjunctival epithelium anteriorly; lack of expression posteriorly
38/39	Onset of mineralization	Homogeneous vascular network throughout sclera; all avascular zones obliterated	Lack of expression anteriorly and posteriorly

References

- Adams, J.C. & Lawler, J. 2011. The thrombospondins. *Cold Spring Harb Perspect Biol.* **3**, a009712.
- Amarilio, R., Viukov, S. V., Sharir, A., Eshkar-Oren, I., Johnson, R. S., Zelzer, E. 2007. HIF1 α regulation of *Sox9* is necessary to maintain differentiation of hypoxic prechondrogenic cells during early skeletogenesis. *Development.* **134**, 3917-3928.
- Araldi, E. & Schipani, E. 2010. Hypoxia, HIFs and bone development. *Bone.* **47**(2), 190-196.
- Argraves, W. S., Larue, A. C., Fleming, P. A., Drake, C. J. 2002. VEGF signaling is required for the assembly but not the maintenance of embryonic blood vessels. *Dev Dyn.* **225**, 298-304.
- Atchley, W. R. & Hall, B. K. 1991. A model for development and evolution of complex morphological structures. *Biol Rev.* **66**, 101-157.
- Barriga, E. H., Maxwell, P. H., Reyes, A. E., Mayor, R. 2013. The hypoxia factor Hif-1 α controls neural crest chemotaxis and epithelial to mesenchymal transition. *J Cell Biol.* **201**(5), 759-776.
- Bentovim, L., Amarilio, A. & Zelzer, E. 2013. HIF1 α is a central regulator of collagen hydroxylation and secretion under hypoxia during bone development. *Development.* **140**, 4473-4483.
- Bornstein, P. 2009. Thrombospondins function as regulators of angiogenesis. *J Cell Commun Signal.* **3**, 189-200.
- Brady, J. 1965. A simple technique for making very fine, durable dissecting needles by sharpening tungsten wire electrolytically. *Bull World Health Organ.* **32**(1), 143-144.
- Byun, J. H., Park, B. W., Kim, J. R., Lee, J. H. 2007. Expression of vascular endothelial growth factor and its receptors after mandibular distraction osteogenesis. *Int J Oral Maxillofac Surg.* **36**, 338-344.

- Carroll, V. A. & Ashcroft, M. 2005. Targeting the molecular basis for tumour hypoxia. *Expert Rev Mol Med.* **7**, 1-16.
- Coelho, C. N. & Kosher, R. A. 1991. Gap junctional communication during limb cartilage differentiation. *Dev Biol.* **144**(1), 47-53.
- Coulombre, A. J., Coulombre, J. L. & Mehta, H. 1962. The skeleton of the eye I. Conjunctival papillae and scleral ossicles. *Dev Biol.* **5**, 382-401.
- Coultas, L., Chawengsaksophak, K. & Rossant, J. 2005. Endothelial cells and VEGF in vascular development. *Nature.* **438**, 937-945.
- Dabelow, A. 1927. Der Scleralring der Sauropsiden, sein phylogentischer Ursprung und seine ontogenetische Entwicklung. *Z Morphol Anthropol.* **26**, 305-332.
- Deckers, M. M. L., Karperien, M., van der Bent, C., Yamashita, T., Papapoulos, S., Löwik, C. W. G. M. 2000. Expression of vascular endothelial growth factors and their receptors during osteoblast differentiation. *Endocrinology* **141**, 1667-1674.
- De Spiegelaere, W., Cornillie, P., Casteleyn, C., Burvenich, C., Van den Broeck, W. 2010. Detection of hypoxia inducible factors and angiogenic growth factors during foetal endochondral and intramembranous ossification. *Anat Histol Embryol.* **39**, 376-384.
- Duench, K. & Franz-Odenaal, T. A. 2012. BMP and Hedgehog signaling during the development of scleral ossicles. *Dev Biol.* **365**(1), 251-258.
- Dunlop, L. T. & Hall, B. K. 1995. Relationships between cellular condensation, preosteoblast formation and epithelial-mesenchymal interactions in initiation of osteogenesis. *Int J Dev Biol.* **39**, 357-371.
- Ede, D. A. & Kelly, W. A. 1964. Developmental abnormalities in the trunk and limbs of the *talpid*³ mutant of the fowl. *J Embryol exp Morph.* **12**, 339-356.
- Edsall, S. C. & Franz-Odenaal, T. A. 2010. A quick whole-mount protocol for bone deposition and resorption. *Zebrafish.* **7**, 275-280.

Eshkar-Oren, I., Viukov, S. V., Salameh, S., Krief, S., Oh, C., Akiyama, H., et al. 2009. The forming limb skeleton serves as a signaling center for limb vasculature patterning via regulation of *Vegf*. *Development* **136**, 1263-1272.

Evans, D. J. R. & Noden, D. M. 2006. Spatial relations between avian craniofacial neural crest and paraxial mesoderm cells. *Dev Dyn.* **235**, 1310-1325.

Fitch, N. 1957. An embryological analysis of two mutants in the house mouse, both producing cleft palate. *J Exp Zool.* **136**(2), 329-361.

Franz-Odendaal, T. A., Hall, B. K. & Witten, P. E. 2006. Buried alive: How osteoblasts become osteocytes. *Dev Dyn.* **235**, 176-190.

Franz-Odendaal, T. A., Ryan, K. & Hall, B. K. 2007. Developmental and morphological variation in the teleost craniofacial skeleton reveals an unusual mode of ossification. *J Exp Zool Mol Dev Evol.* **3088**, 709-721.

Franz-Odendaal, T. A. 2008. Toward understanding the development of scleral ossicles in the chicken, *Gallus gallus*. *Dev Dyn.* **237**, 3240-3251.

Franz-Odendaal, T. A. 2011a. Induction and patterning of intramembranous bone. *Front. Biosci.* **17**, 3723-3746.

Franz-Odendaal, T. A. 2011b. Epigenetics in Bone and Cartilage Development. In Hallgrímsson, B. & Hall, B. K. (Eds.), *Epigenetics: Linking genotype and phenotype in development and evolution* (pp 195-220). Berkeley, CA. University of California Press.

Garol, J. D., Fields Jr., H. W., Metzner, L., Kokich, V. G. 1978. The craniofacial skeleton in anencephalic human fetuses. II. Calvarium. *Teratology* **17**(1), 67-73.

Gendron-Maguire, M., Mallo, M., Zhang, M., Gridley, T. 1994. *Hoxa-2* mutant mice exhibit homeotic transformation of skeletal elements derived from cranial neural crest. *Cell.* **75**, 1317-1331.

Grüneberg, H. 1963. The pathology of development: a study of inherited skeletal disorders in animals. Blackwell, Oxford.

- Hall, B. K. 1975. Evolutionary consequences of skeletal differentiation. *Amer Zool.* **15**(2), 329-350.
- Hall, B. K. 1981. Specificity in the differentiation and morphogenesis of neural crest-derived scleral ossicles and of epithelial scleral papillae in the eye of the embryonic chick. *J. Embryol. Exp. Morph.* **66**, 175-190.
- Hall, B. K. & Herring, S. W. 1990. Paralysis and growth of the musculoskeletal system in the embryonic chick. *J Morphol.* **206**(1), 45-56.
- Hall, B. K. & Miyake, T. 1992. The membranous skeleton: the role of cell condensations in vertebrate skeletogenesis. *Anat Embryol.* **186**, 107-124.
- Hall, B. K. & Miyake, T. 1995. Divide, accumulate, differentiate: cell condensation in skeletal development revisited. *Int J Dev Biol.* **39**, 881-893.
- Hall, B. K. & Miyake, T. 2000. All for one and one for all: condensations and the initiation of skeletal development. *BioEssays.* **22**, 138-147.
- Hamburger, V. & Hamilton, H. L. A series of normal stages in the development of the chick embryos. *J Morphol.* **88**(1), 49-92.
- Jabalee, J., Hillier, S. & Franz-Odenaal, T. A. 2013. An investigation of cellular dynamics during the development of intramembranous bones: the scleral ossicles. *J Anat.* **223**, 311-320.
- Jacobsen, K. A., Al-Aql, Z. S., Wan, C., Fitch, J. L., Stapleton, S. N., Mason, Z. D. et al. 2008. Bone formation during distraction osteogenesis is dependent on both VEGFR1 and VEGFR2 signaling. *J Bone Miner Res.* **23**(5), 596-609.
- Jeffery, G. 2001. Architecture of the optic chiasm and the mechanisms that sculpt its development. *Physiol Rev.* **81**, 1393-1414.
- Jiang, X., Iseki, S., Maxson, R. E., Sucov, H. M., Morriss-Kay, G. M. 2002. Tissue origins and interactions in the mammalian skull vault. *Dev Biol.* **241**, 106-116.

- Jourdeuil, K. & Franz-Odenaal, T. A. 2012. Vasculogenesis and the induction of skeletogenic condensations in the avian eye. *Anat. Rec.* **295**, 691-698.
- Jung, J., Tiwari, A., Inamadar, S. M., Thomas, C. P., Goel, A., Choudhury, A. 2012. Secretion of soluble vascular endothelial growth factor receptor (sVEGFR1/sFLT1) requires Arf1, Arf6, and Rab11 GTPases. *PLoS One.* **7**(9), e44572.
- Kendall, R. L., Wang, G. & Thomas, K. A. 1996. Identification of a natural soluble form of the vascular endothelial growth factor receptor, FLT-1, and its heterodimerization with KDR. *Biochem Biophys Res Commun.* **226**, 324-328.
- Killer, H. E., Jaggi, G. P., Flammer, J., Miller, N. R., Huber, A. R., Mironov, A. 2007. Cerebrospinal fluid dynamics between the intracranial and the subarachnoid space of the optic nerve. Is it always bidirectional? *Brain.* **130**, 514-520.
- Kusumbe, A. P., Ramasamy, S. K. & Adams, R. H. 2014. Coupling of angiogenesis and osteogenesis by a specific vessel subtype in bone. *Nature.* **507**, 323-328.
- Kwiatkowski, S., Munjaal, R. P., Lee, T., Lwigale, P. Y. 2013. Expression of pro- and anti-angiogenic factors during the formation of the periocular vasculature and development of the avian cornea. *Dev Dyn.* **242**(6), 738-751.
- Liu, Y., Berendsen, A. D., Jia, S., Lotinun, S., Baron, R., Ferrara, N. et al. 2012. Intracellular VEGF regulates the balance between osteoblast and adipocyte differentiation. *J Clin Invest.* doi:10.1172/JC161209.
- Liu, Y. & Olsen, B. R. 2014. Distinct VEGF functions during bone development and homeostasis. *Arch Immunol Ther Exp.* doi 10.1007/s00005-014-0285-y.
- MacDonald, M. E. & Hall, B. K. 2001. Altered timing of the extracellular-matrix-mediated epithelial-mesenchymal interaction that initiates mandibular skeletogenesis in three inbred strain of mice: Development, heterochrony, and evolutionary change in morphology. *J Exp Zool.* **291**(3), 258-273.
- Maes, C., Kobayashi, T., Selig, M. K., Torrekens, S., Roth, S. I., Mackem, S. et al. 2010. Osteoblast precursors, but not mature osteoblasts, move into developing and fractured bones along with invading blood vessels. *Dev Cell.* **19**, 329-244.

Maes, C., Araldi, E., Haigh, K., Khatri, R., Van Looveren, R., Giaccia, A. J. et al. 2012. VEGF-independent cell-autonomous functions of HIF-1 α regulating oxygen consumption in fetal cartilage are critical for chondrocyte survival. *J Bone Miner Res.* **27**(3), 596-609.

Mammoto, T., Akiko, M., Torisawa, Y., Tat, T., Gibbs, A., Derda, R. et al. 2011. Mechanochemical control of mesenchymal condensation and embryonic tooth organ formation. *Dev Cell.* **21**(4), 758-769.

Mayer, H., Bertram, H., Lindenmaier, W., Korff, T., Weber, H., Weich, H. 2005. Vascular endothelial growth factor (VEGF-A) expression in human mesenchymal stem cells: Autocrine and paracrine role on osteoblastic and endothelial differentiation. *J Cell Biochem.* **95**, 827-839.

Mayr-Wohlfart, U., Waltenberger, J., Hausser, H., Kessler, S. Günther, K. P., Dehio, C. et al. 2002. Vascular endothelial growth factor stimulates chemotactic migration of primary human osteoblasts. *Bone.* **30**(3), 472-477.

Meadows, S. M., Fletcher, P. J., Moran, C., Xu, K., Neufeld, G., Chauvet, S., et al. 2012. Integration of repulsive guidance cues generates avascular zones that shape mammalian blood vessels. *Circ Res.* **110**, 34-36.

Meury, T., Verrier, S. & Mauro, A. 2006. Human endothelial cells inhibit BMSC differentiation into mature osteoblasts in vitro by interfering with osterix expression. *J Cell Biochem.* **98**(4), 992-1006.

Midy, V. & Plouët, J. 1994. Vasculotropin/Vascular endothelial growth factor induces differentiation in cultured osteoblasts. *Biochem Biophys Res Commun.* **199** (1), 380-386.

Murray, P. D. F. 1941. Epidermal papillae and dermal bones of the chick sclerotic. *Nature.* **148**, 471.

Murray, P. D. F. 1943. The development of the conjunctival papillae and of the scleral bones in the embryo chick. *J Anat.* **77**, 225-240.

Myllyharju, J. & Schipani, E. 2010. Extracellular matrix genes as hypoxia-inducible targets. *Cell Tissue Res.* **339**, 19-29.

Nieto, M. A., Patel, K. & Wilkinson, D. G. 1996. In situ hybridization of chick embryos in whole mount and tissue sections. *Methods Cell Biol.* **51**, 219-235.

Noden, D. M. & Trainor, P. A. 2005. Relations and interactions between cranial mesoderm and neural crest populations. *J Anat.* **207**, 575-601.

Nussbaum, M. 1901. Zur Rückbildung embryonaler Anlagen. *Arch mikroskop Anat.* **57**, 676-705.

Pacicca, D. M., Patel, N., Lee, C., Salisbury, K., Lehmann, W., Carvalho, R. et al. 2003. Expression of angiogenic factors during distraction osteogenesis. *Bone.* **33**, 889-898.

Palumbo, C., Cavani, F., Sena, P., Benincasa, M., Ferretti, M. 2012. Osteocyte apoptosis and absence of bone remodeling in human auditory ossicles and scleral ossicles of lower vertebrates: A mere coincidence or linked processes? *Calcif Tissue Int.* **90**, 211-218.

Park, J. H., Park, B. H., Kim, H. K., Park, T. S., Baek, H. S. 2002. Hypoxia decreases Runx2/Cbfa1 expression in human osteoblast-like cells. *Mol Cell Endocrinol.* **192**, 197-203.

Percival, C. J. & Richtsmeier, J. T. 2013. Angiogenesis and intramembranous osteogenesis. *Dev Dyn.* **242**(8), 909-922.

Pinto, C. B. & Hall, B. K. 1991. Toward an understanding of the epithelial requirement for osteogenesis in scleral mesenchyme of the embryonic chick. *J Exp Zool.* **259**, 92-108.

Provot, S., Zinyk, D., Gunes, Y., Kathri, R., Le, Q., Kronenberg, H. M. et al. 2007. Hif-1 α regulates differentiation of limb bud mesenchyme and joint development. *J Cell Biol.* **177**(3), 451-464.

Ramasamy, S. K., Kusumbe, A. P., Wang, L., Adams, R. H. 2014. Endothelial Notch activity promotes angiogenesis and osteogenesis in bone. *Nature.* **507**, 376-380.

Riddle, R. C., Lakhanpai, A. & Clemens, T. L. 2010. Role of vessel growth factors in bone development and repair. *Joint Bone Spine.* **77**, 517-518.

- Rijli, F. M., Mark, M., Lakkaraju, S., Dierich, A., Dollé, P., Chambon, P. A. 1994. Homeotic transformation is generated in the rostral branchial region of the head by disruption of *Hoxa-2*, which acts as a selector gene. *Cell*. **75**, 1333–1349.
- Robinson, C. J. & Stringer, S. E. 2001. The splice variants of vascular endothelial growth factor (VEGF) and their receptors. *J Cell Sci*. **114**, 853-865.
- Rot-Nikcevic, I., Reddy, T., Downing, K. J., Belliveau, A. C., Hallgrímsson, B., Hall, B. K. et al. *Myf5^{-/-}:MyoD^{-/-}* amyogenic fetuses reveal the importance of early contraction and static loading by striated muscle in mouse skeletogenesis. *Dev Genes Evol*. **216**(1), 1-9.
- Salim, A., Nacamuli, R. P., Morgan, E. F., Giaccia, A. J., Longaker, M. T. 2004. Transient changes in oxygen tension inhibit osteogenic differentiation and *runx2* expression in osteoblasts. *J Biol Chem*. **279** (38), 40007-40016.
- Schipani, E., Ryan, H. E., Didrickson, S., Kobayashi, T. Knight, M. Johnson, R. S. Hypoxia in cartilage: HIF-1 α is essential for chondrocyte growth arrest and survival. *Genes Dev*. **15**, 2865-2876.
- Schmidt, M. & Flamme, I. 1998. The in vivo activity of vascular endothelial growth factor isoforms in the avian embryos. *Growth Factors*. **15**(3), 183-197.
- Shibuya, M. 2001. Structure and dual function of vascular endothelial growth factor receptor-1 (Flt-1). *Int J Biochem Cell Biol*. **33**(4), 409-420.
- Simunovic, F., Steiner, D., Pfeifer, D., Stark, G. B., Finkenzeller, G., Lampert, F. 2013. Increased extracellular matrix and proangiogenic factor transcription in endothelial cells after cocultivation with primary human osteoblasts. *J Cell Biochem*. **114**(7), 1584-1594.
- Steinbrech, D. S., Mehrara, B. J., Saadeh, P. B., Greenwald, J. A., Spector, J. A., Gittes, G. K. et al. 2000. VEGF expression in an osteoblast-like cell line is regulated by a hypoxia response mechanism. *Am J Physiol Cell Physiol*. **278**, C853-C860.
- Stern, C. D. 2005. The chick: A great model system becomes even greater. *Dev Cell*. **8**(1), 9-17.

Street, J. & Lenehan, B. 2009. Vascular endothelial growth factor regulates osteoblast survival – evidence for an autocrine feedback mechanism. *J Orthop Surg Res.* **4**:19. doi:10.1186/1749-799X-4-19

Takahashi, Y., Sipp, D. & Enomoto, H. 2013. Tissue interactions in neural crest cell development and disease. *Science.* **341**, 860-863.

Takase, Y., Tadokoro, R. & Takahashi, Y. 2013. Low cost labeling with highlighter ink efficiently visualizes developing blood vessels in avian and mouse embryos. *Develop Growth Differ.* **55**, 792-801.

Theveneau, E. & Mayor, R. 2012. Neural crest migration: interplay between chemorepellants, chemoattractants, contact inhibition, epithelial-mesenchymal transition, and collective cell migration. *WIREs Dev Biol.* **1**, 435-445.

Thompson, T. J., Owens, P. D. A & Wilson, D. J. 1989. Intramembranous osteogenesis and angiogenesis in the chick embryo. *J Anat.* **166**, 55-65.

Tucker, R. P., Adams, J. C. & Lawler, J. 1995. Thrombospondin-4 is expressed by early osteogenic tissues in the chick embryo. *Dev Dyn.* **203**, 477-490.

Utting, J. C., Robins, S. P., Brandao-Burch, A., Orriss, I. R., Arnett, T. R. 2006. Hypoxia inhibits the growth, differentiation and bone-forming capacity of rat osteoblasts. *Exp Cell Res.* **312**, 1693-1702.

von Schroeder, H. P., Veillette, C. J., Payandeh, J., Qureshi, A., Heersche, J. N. M. 2003. Endothelin-1 promotes osteoprogenitor proliferation and differentiation in fetal rat calvarial cell cultures. *Bone.* **33**, 673-684.

Walls, G. L. (Editor). 1942. The vertebrate eye and its adaptive radiation. Bloomfield Hills, MI, Cranbrook Institute of Science.

Wan, C., Gilbert, S. R., Wang, Y., Cao, X., Shen, X., Ramaswamy, G. et al. 2008. Activation of the hypoxia-inducible factor-1 pathway accelerates bone regeneration. *PNAS.* **105**(2), 686-691.

Wang, Y., Wan, C., Deng, L., Liu, X., Cao, X., Gilbert, S. R., et al. 2007. The hypoxia-inducible factor α pathway couples angiogenesis to osteogenesis during skeletal development. *J Clin Invest.* **117**(6), 1616-1626.

Wilson, K. Investigations into the avian scleral ossicle system using fluorescent dye labeling and alkaline phosphatase staining. (Honours thesis). Mount Saint Vincent University: Canada.

Yamaguchi, S., Iwata, K. & Shibuya, M. 2002. Soluble Flt-1 (soluble VEGFR-1), a potent natural antiangiogenic molecule in mammals, is phylogenetically conserved in avians. *Biochem Biophys Res Commun.* **291**, 554-559.

Yang, W., Guo, D., Harris, M. A., Cui, Y., Gluhak-Heinrich, J., Wu, J. et al. 2013. *Bmp2* in osteoblasts of periosteum and trabecular bone links bone formation to vascularization and mesenchymal stem cells. *J Cell Sci.* **126**, 4085-4098.

Yin, M. & Pacifici, M. 2001. Vascular regression is required for mesenchymal condensation and chondrogenesis in the developing limb. *Dev Dyn.* **222**, 522-533.

Yin, M., Gentili, C., Koyama, E., Zasloff, M., Pacifici, M. 2002. Antiangiogenic treatment delays chondrocyte maturation and bone formation during limb skeletogenesis. *J Bone Miner Res.* **17**(1), 56-65.

Zelzer, E., Glotzer, D. J., Hartmann, C., Thomas, D., Fukai, N., Soker, S. et al. 2001. Tissue specific regulation of VEGF expression during bone development requires *Cbfa1/Runx2*. *Mech Dev.* **106**, 97-106.

Zelzer, E., McLean, W., Ng, Y., Fukai, N., Reginato, A. M., Lovejoy, S. et al. 2002. Skeletal defects in VEGF^{120/120} mice reveal multiple roles for VEGF in skeletogenesis. *Development.* **129**, 1893-1904.

Zelzer, E., Mamluk, R., Ferrara, N., Johnson, R. S., Schipani, E., Olsen, B. R. 2004. VEGFA is necessary for chondrocyte survival during bone development. *Development and Disease.* **131**(9), 2161-2171.

Zhang, G., Boyle, D. L., Zhang, Y., Rogers, A. R., Conrad, G. W. 2012. Development and mineralization of embryonic avian scleral ossicles. *Mol Vis.* **18**, 348-361.

Appendix A - Preparing LB Broth and Agar Plates

LB broth (2.5% LB in dH₂O; 100 ml)

2.5 g LB (BD, 244620)

100 ml dH₂O

Autoclave

Agar plates (2.5% LB, 1.5% agar, 0.01% ampicillin in dH₂O; 250 ml)

6.25 g LB

3.75 g agar (BD, 214530)

250 ml dH₂O

Heat with stirring until agar has dissolved.

Cover flask with tin foil, autoclave

Cool agar

Add 0.025 g ampicillin (Sigma, A6140)

Pour solution into plates and allow to harden

Parafilm and store plates upside down at 4°C

Appendix B - Cloning

Day 1

Remove competent *E. coli* cells (Promega, L1011) from -80°C freezer and thaw on ice.

Gently mix the thawed cells then pipette 100 µl of bacteria into each chilled Nalgene tube using a chilled pipette tip.

Add 10 µl DNA from filter paper to experimental tube and 10 µl TE buffer to control tube.

Incubate tubes on ice 10 – 20 minutes.

Heat shock tubes for 45 – 50 seconds in a 42°C water bath.

Incubate tubes on ice 2 minutes.

Add 900 µl cold LB broth to each tube using a chilled tip. Incubate tubes 60 minutes at 37°C with shaking.

Dispense of cells onto plates. Incubate at 37°C overnight.

Day 2

Flame edge of LB bottle and tube before pouring a small amount of LB into Nalgene tube. Make one tube per plate or choose best plate.

Use a sterile pipette tip to scoop an isolated bacterial colony. Throw the tip containing the colony into the tube and close the tube. Repeat for each plate.

Incubate plates overnight at 37°C with shaking.

Day 3 (Minipreparation)

Take 2 ml from each overnight culture and place in an Eppendorf tube. Centrifuge at 13,000 rpm for 1 minute. Repeat twice to increase pellet size. Store overnight cultures in the fridge.

Pour off supernatant. Keep pellet.

Add 250 μ l cold buffer #1 to tube. Re-suspend pellet by dragging tube over racks.

Add 250 μ l cold fresh lysis solution. Mix by inverting and incubate on ice 5 minutes.

Add 250 μ l cold potassium acetate and mix until solution turns cloudy. Incubate on ice 5 minutes.

Centrifuge at 13,000 rpm 5 minutes. Pour supernatant into a new tube. Discard flocculent white waste.

In the fume hood, add 200 μ l phenol-chloroform and shake 30 seconds.

Centrifuge at 13,000 rpm 5 minutes. Remove top layer with a pipette and dispense into new tube. Dispose of bottom layer.

Add an equal volume of isopropanol. Mix by inversion 30 seconds. Incubate at room temperature 2 minutes.

Centrifuge at 13,000 rpm 5 minutes. Carefully decant the supernatant.

Add 200 μ l cold 95% ethanol to each tube, invert, and centrifuge at 13,000 rpm 5 minutes. Discard supernatant.

Allow pellet to dry on bench (approx. 10 minutes).

Re-suspend pellet in 50 μ l DEPC H₂O. Remove 2 μ l and store for gel electrophoresis.

Continue with digestion or store at -20.

Recipes:

Buffer #1 (50 mM Tris-Cl, 10 mM EDTA, 100 μ g/ml ribonuclease A in dH₂O; 1 ml)

50 μ l 1 M Tris-Cl (pH 8.0)

10 μ l 1 M EDTA (Sigma, E5134)

100 μ g ribonuclease A (Sigma, R4642)

Top up to 1 ml with dH₂O

Lysis buffer (200 mM NaCl, 1% SDS in dH₂O; 1 ml)

100 μ l 2 M NaCl (EMD Millipore, SX0420)

100 μ l 10% SDS (Sigma, L4390)

Top up to 1 ml with dH₂O

Appendix C - Digestion and Clean-Up of Plasmid DNA

Digestion

In a small RNase-free Eppendorf tube, combine the following reagents:

- DNA from minipreparation (no more than 10 µg)
- 5 µl restriction endonuclease (NotI for antisense; SalI for sense)
- 5 µl buffer (specific to the endonuclease used)
- 10 µl 0.1 mg/ml BSA
- 70 µl DEPC H₂O

Incubate at 37°C overnight.

Heat inactivate digest at 65°C 15 minutes.

Clean-up

Clean-up was done using a High Pure PCR product purification kit (Roche, 11 732).

Add 500 µl binding buffer to sample and mix well.

Insert one High Pure filter tube into a collection tube. Transfer sample to upper reservoir of filter tube and centrifuge 13,000 rpm 1 minute.

Discard flowthrough. Reconnect filter tube.

Add 500 µl binding buffer to the upper reservoir. Centrifuge 13,000 rpm 1 minute.

Discard flowthrough. Reconnect filter tube.

Add 200 µl wash buffer to the upper reservoir. Centrifuge 13,000 rpm 1 minute.

Discard flowthrough. Connect new, clean Eppendorf tube.

Add 50 µl elution buffer to the upper reservoir. Centrifuge 13,000 rpm 1 minute. This is elution 1. Repeat with a new tube. This is elution 2.

Appendix D - Probe Preparation

Probe preparation was carried out using a DIG-RNA labelling kit (Roche, 11 175 025

910) according to the manufacturer's instructions as follows:

Combine the following reagents in a 0.2 ml PCR tube

- 1 µg DNA from elution
- 2 µl DIG RNA labelling mix
- 2 µl 10x transcription buffer
- 1 µl protector RNase inhibitor
- 2 µl polymerase (T3 for antisense; T7 for sense)
- Top up to 20 µl with DEPC H₂O

Incubate at 37°C 2 hours.

Add 2 µl DNase I.

Incubate at 37°C 15 minutes.

Stop reaction by adding 2 µl 0.2 M EDTA (pH 8.0).

Remove 1 µl from tube and place in a new 0.2 ml PCR tube. This is 'tube 1' of the dot blot dilution series (see below).

Appendix E - Dot Blot

Test 1 μ l antisense and sense probes against positive control RNA. To do so, make a dilution series of varying probe concentrations in dilution buffer (Table 1).

Blot 1 μ l from each tube in the dilution series onto a nitrocellulose membrane (Roche, 11 209 299 001).

Bake membrane at 120°C 30 minutes to adhere nucleic acids to membrane.

Place membrane in a petri dish and incubate in the following solutions:

- Maleic acid buffer 2 minutes
- Blocking buffer 20 minutes
- 1x TBST 5 minutes
- Antibody solution 30 minutes
- Washing buffer 2x15 minutes
- Detection buffer 5 minutes

Add color detection buffer and incubate in the dark.

Check membrane every 30 seconds up to 5 minutes for the appearance of dots.

After the initial 5 minutes, check every subsequent 5 minutes.

To stop the reaction, incubate membrane in TE buffer 5 minutes.

Store membrane dry, in the dark.

Table 1 – RNA dilution series for dot blot

Tube #	RNA (μl)	Dilution buffer (μl)	From previous tube (μl)	Final [RNA]
1	1	40.6	-	10 ng/ μ l
2	-	18	2 from tube 1	1 ng/ μ l
3	-	198	2 from tube 2	10 pg/ μ l
4	-	35	15 from tube 3	3 pg/ μ l
5	-	45	5 from tube 3	1 pg/ μ l

Recipes:

Dilution buffer (5:3:2 DEPC H₂O:SSC:formaldehyde; 0.5 ml)

100 μ l formaldehyde (Sigma, F8775)

150 μ l 20x SSC (Sigma, S6639)

250 μ l DEPC H₂O

Maleic acid buffer (0.1 M maleic acid, 0.15 M NaCl in DEPC H₂O; 100 ml)

1.1607 g maleic acid (Fisher Scientific, 03417)

0.8766 g NaCl (EMD Millipore, SX0420)

pH to 7.5 with DEPC-treated solutions (HCl, NaOH)

Top up to 100 ml with DEPC H₂O

Blocking solution (2% sheep serum, 3% milk powder in 1x TBST; 10 ml)

0.2 ml sheep serum (Sigma, S3772)

0.3 g milk powder

10 ml 1x TBST

Antibody solution (1:5000 anti-DIG AP Fab fragments: 1x TBST; 10 ml)

2 µl anti-DIG-AP Fab fragments (Roche, 11 093 274 910)

10 ml 1x TBST

Washing buffer (0.1 M maleic acid, 0.15 M NaCl, 0.3% TWEEN 20; 100 ml)

1.1607 g maleic acid

0.8766 g NaCl

pH to 7.5 with DEPC-treated solutions

Top up to 100 ml with DEPC H₂O

0.3 ml TWEEN 20 (Sigma, P9416)

Detection buffer (0.1 M Tris-Cl, 0.1 M NaCl in DEPC H₂O; 100 ml)

10 ml 1 M Tris-Cl

0.5844 g NaCl

Top up to 100 ml with DEPC H₂O

Color detection buffer (0.15 mg/ml BCIP, 0.30 mg/ml NBT in dH₂O; 10 ml)

1 SIGMAFAST BCIP/NBT tablet (Sigma, B5655)

10 ml dH₂O

Shake until dissolved (in the dark)

TE buffer (10 mM Tris-Cl, 1 mM EDTA, pH 8.0; 100 ml)

1 ml 1 M Tris-Cl

0.2 ml 0.5 M EDTA (Sigma, E5134)

pH to 8.0 with DEPC-treated solutions

Top up to 100 ml with DEPC H₂O

Appendix F - Whole Mount In Situ Hybridization

Day 1 - Fixation

Fix embryos in 4% PFA/1x PBST at 4°C overnight.

Day 2 - Dehydration

Wash embryos 2 x 10 minutes in 1x PBST on ice with shaking.

Dehydrate embryos through a graded MeOH series on ice with shaking in the following solutions (30 – 60 minutes per solution, depending on stage):

- 12.5/87.5% MeOH/1x PBST
- 25/75% MeOH/1x PBST
- 50/50% MeOH/1x PBS
- 75/25% MeOH/DEPC H₂O
- 85/15% MeOH/DEPC H₂O
- Store embryos in 100% MeOH at -20°C for at least one overnight or as long as required.

Day 3 - Rehydration

Sometime prior to running the in situ, bisect the heads, remove the vitreous humor and lens and dissect off eyelids and the nictitating membrane.

Rehydrate embryos through a graded MeOH series at room temperature with shaking in the following solutions (30 minutes per solution or until head has sunk):

- 85/15% MeOH/DEPC H₂O at room temp. with shaking until embryo sinks
- 75/25% MeOH/DEPC H₂O at room temp. with shaking until embryo sinks

- 50/50% MeOH/1x PBS at room temp. with shaking until embryo sinks
- 25/75% MeOH/1x PBST at room temp. with shaking until embryo sinks
- 12.5/87.5% MeOH/1x PBST at room temp. with shaking until embryo sinks

Wash 2 x 10 minutes in 1x PBST at room temperature with shaking.

Bleach overnight 10% Hydrogen Peroxide/1x PBST at room temperature with shaking.

Day 4 - Hybridization

Wash 2 x 10 minutes in 1x PBST at room temperature with shaking.

Digest 30 - 60 minutes in 50µg/ml ProK/1x PBST at room temperature with shaking.

Post-fix 20 minutes in 2% PFA/1x PBST + 0.25% glutaraldehyde/1xPBS (50:50) at room temperature with shaking.

Wash 2 x 10 minutes in 1x PBST at room temperature with shaking.

Put embryos in pre-warmed prehyb containing fresh heparin and yeast tRNA at 60°C with shaking for 2 hours.

To fresh, pre-warmed prehyb, add desired concentration of probe. Incubate embryos in probe solution overnight at 60°C with gentle shaking.

Day 5 – Probe detection

Wash 3 x 20 minutes in pre-warmed Wash I at 60°C with shaking.

Wash 3 x 20 minutes in pre-warmed Wash II at 60°C with shaking.

Wash 3 x 10 minutes in 1x TBST at room temperature with shaking.

Block 2 hours in 20% sheep serum/1x TBST (heat inactivated) at 4°C with shaking.

Pre-absorb antibody as follows:

- Combine 1ml of 20% sheep serum/1x TBST (heat inactivated) with 1 μ l anti-DIG-AP Fab fragments (Roche, 11 093 274 910) and a tiny amount of embryo powder in an Eppendorf tube.
- Shake tube vigorously.
- Let powder settle for 30 minutes on ice.
- Remove the antibody and add it to the rest of the 20% inactivated sheep serum/1x TBST to make the correct dilution [1 μ l preabsorbed anti-DIG-AP Fab fragments per 10 ml 20% sheep serum/1xTBST (heat inactivated)].

Add antibody solution to embryos and incubate overnight at 4°C with shaking.

Day 6 -8 – Background reduction

Wash 3 x 10 minutes in 1x TBST at room temperature with shaking.

Reduce background by washing embryos in 1x TBST + 2mM levamisole at 4°C with shaking. Change 1x TBST + 2 mM levamisole 1 -3 times/day over a 2 – 3 day period.

Day 9 – Color detection

Wash 3 x 10 minutes 1x NTMT + 2mM levamisole at room temperature with shaking.

Make color solution by dissolving one SIGMAFAST BCIP/NBT tablet in 10 ml 10% PVA/1x NTMT.

Incubate embryos in color solution in glass vials in the dark at room temperature with gentle shaking until developed (typically 24 hours).

Day 10 - Storage

Stop color reaction by washing embryos 3 x 10 minutes in 1X PBST + 5mM EDTA at room temperature without shaking.

Postfix in 4% PFA/1x PBST for 60 minutes at room temperature without shaking.

Wash 2 x 10 minutes in 1X PBST at room temperature without shaking.

Leech background in 90% MeOH at 4°C without shaking. Watch reaction to ensure no loss of specific staining. This may take from a few minutes to overnight.

Quickly rinse in dH₂O and store in 50:50 dH₂O/glycerol at 4°C.

Recipes:

0.1% DEPC-treated water (1L)

1L dH₂O

1 ml DEPC (Sigma, D5758)

Shake vigorously 30 minutes

Let stand in fumehood with top cracked for at least one hour

Autoclave

10x PBST (137 mM NaCl, 2.5 mM KCl, 4.3 mM Na₂HPO₄, 1.4 mM KH₂PO₄, 1% TWEEN 20 in DEPC H₂O; 500 ml)

137 ml 5 M NaCl (EMD Millipore, SX0420)

3.37 ml 4 M KCl (MP Biomedicals, 191427)

21.5 ml 1 M Na₂HPO₄ (EMD Millipore, SX0720)

7 ml 1 M KH₂PO₄ (Sigma, P5655)

Top up to $\frac{3}{4}$ volume with DEPC H₂O

pH to 7.4 using DEPC-treated solutions (HCl, NaOH)

5 ml TWEEN 20 (Sigma, P9416)

Top up to 500 ml with DEPC H₂O

10% Hydrogen peroxide/1x PBST (25 ml)

6.67 ml H₂O₂ stock (30%; VWR, BOH3742-1)

13.3 ml 1x PBST

50 µg/ml Proteinase K (ProK) (25 ml)

125 µl ProK stock (10 mg/ml; Sigma, P2308)

25ml 1x PBST

2% PFA/1x PBST + 0.25% glutaraldehyde/PBS (25 ml)

12.5 ml 4% PFA in 1x PBST

125 µl stock glutaraldehyde (25%) in 12.5 ml 1x PBS

Prehyb (50% deionized formamide, 5x SSC, 1% SDS, 50 µg/ml heparin, 50 µg/ml RNA in DEPC H₂O; 30 ml)

15 ml formamide (Amresco, 0606)

7.5 ml 20x SSC (Sigma, S6639)

3 ml 10% SDS

4.5 ml DEPC H₂O

0.0015 g heparin sodium salt from porcine intestinal mucosa (Sigma, H3393)

0.0015 g RNA from yeast (Roche, 10 109 223 001)

Wash I (50% deionized formamide, 4x SSC, 1% SDS in DEPC H₂O; 50 ml)

25 ml deionized formamide

10 ml 20x SSC

5 ml 10% SDS

Top up to 50 ml with DEPC H₂O

Wash II (50% deionized formamide, 2x SSC in DEPC H₂O; 50 ml)

25 ml deionized formamide

5 ml 20x SSC

20 ml DEPC H₂O

*10x TBST (140 mM NaCl, 2.7 mM KCl, 25 mM Tris-Cl, 1% TWEEN 20 in DEPC H₂O;
500 ml)*

140 ml 5 M NaCl

3.37 ml 4 M KCl

125 ml 1 M Tris-Cl (pH 7.5)

5 ml TWEEN 20

Top up to 500 ml with DEPC H₂O

20% Sheep serum/1x TBST (heat inactivated) (25 ml)

5 ml sheep serum (Sigma, S3772)

20 ml 1x TBST

Incubate at 60°C for 30 minutes to inactivate

Chick powder

Collect 4 – 5 day chick embryos in a minimum amount of PBS

Homogenize embryos in a small volume of acetone

Add 4 volumes cold acetone

Incubate on ice 30 minutes

Centrifuge at 10000 rpm 10 minutes

Place embryos on filter paper and crush into a powder

Store at -20°C

1x TBST + 2mM levamisole (25 ml)

0.0121 g (-)-tetramisole hydrochloride (levamisole; Sigma, L9756)

25 ml 1x TBST

*1x NTMT (100 mM NaCl, 100 mM Tris-Cl, 20 mM MgCl₂*6H₂O, 0.1% TWEEN 20 in DEPC H₂O; 100 ml)*

2 ml 5 M NaCl

10 ml 1 M Tris-Cl (pH 9.5)

2 ml 1 M MgCl₂*6H₂O

100 µl TWEEN 20

Top up to 100 ml with DEPC H₂O

1x NTMT + 2 mM levamisole (25 ml)

0.0121 g levamisole

25 ml 1x NTMT

Color solution (10% PVA, 0.15 mg/ml BCIP, 0.30 mg/ml NBT in 1x NTMT; 10 ml)

1 g PVA (Sigma, 348406)

10 ml 1x NTMT

Heat to dissolve PVA

Wrap in foil, cool to room temperature

Dissolve 1 SIGMAFAST BCIP/NBT tablet

Appendix G – Protocol for (3-aminopropyl)triethoxysilane (APTES)-Coated Slides

Wash slides in 100% EtOH

Rinse in tap water

Dry overnight at 36°C, cool

Dip in 2% (3-aminopropyl)triethoxysilane in acetone

Dip in acetone twice

Dip in sterile distilled water

Dry overnight at 36°C

Appendix H – sFlt-1 Implantation Raw Data and Statistical Analysis

Table 2 – Measurement of avascular zone area (μm^2) 1 day post-surgery.

Experiment Number	Treatment	Experimental (right) eye (μm^2)				Control (left) eye (μm^2)			
		1	2	3	Avg	1	2	3	Avg
13-6	sFlt-1	38657.2	40524.7	42789.8	40657.2	21782.7	23657.3	23872.5	23104.1
14-7	sFlt-1	20285.1	19625.0	19555.7	19821.9	15535.6	16080.4	15964.5	15860.1
14-9	sFlt-1	31430.5	32435.0	32962.9	32276.2	23507.5	24109.8	24450.9	24022.7
25-1	sFlt-1	10015.6	11276.0	10759.6	10683.7	14292.2	14187.6	13861.0	14113.6
25-5	sFlt-1	33019.0	31861.1	34224.1	33034.7	10493.5	11623.7	11163.8	11093.7
29-5	sFlt-1	10311.2	10124.8	10876.5	10437.5	7606.0	8140.1	7943.4	7896.5
30-1	sFlt-1	41375.1	42749.6	42935.1	42353.3	35256.8	36489.9	35582.6	35776.4
30-4	sFlt-1	32263.1	30445.2	32862.6	31857.0	19316.5	19523.2	19285.2	19375.0
31-2	sFlt-1	22939.9	20031.1	20015.6	20995.5	17738.2	20978.8	21600.2	20105.8
31-8	sFlt-1	229962.1	232080.7	226947	229663	24882.4	24489.9	23986.7	24453.0
31-9	sFlt-1	70138.64	68048.4	71871.9	70019.7	14307.1	13405.9	14201.6	13971.5
25-2	1x PBS	36211.5	32269.4	34231.0	34237.3	38048.2	36955.9	37469.0	37491.0
30-5	1x PBS	12748.81	12915.99	13016.7	12893.8	16834.2	16628.1	17349.9	16937.4

Experiment Number	Treatment	Experimental (right) eye (μm^2)				Control (left) eye (μm^2)			
		1	2	3	Avg	1	2	3	Avg
30-6	1x PBS	7823.2	7009.0	8224.0	7685.4	5554.6	5460.4	5359.7	5458.3

Table 3 – Measurement of avascular zone area (μm^2) 1 day post-surgery manipulated for statistical analysis.

Experiment Number	Treatment	Difference (Exp-Ctrl)	Difference + constant	Sqrt (difference + constant)
13-6	sFlt-1	17553.1	21606.7	147.0
14-7	sFlt-1	3961.8	8015.4	89.5
14-9	sFlt-1	8253.5	12307.0	111.0
25-1	sFlt-1	-3429.9	623.7	25.0
25-5	sFlt-1	21941.0	25994.6	161.2
29-5	sFlt-1	2541.0	6594.5	81.2
30-1	sFlt-1	6576.8	10630.4	103.1
30-4	sFlt-1	12482.0	16535.6	128.6

Experiment Number	Treatment	Difference (Exp-Ctrl)	Difference + constant	Sqrt (difference + constant)
31-2	sFlt-1	889.7	4943.3	70.3
31-8	sFlt-1	205210.3	209263.9	457.5
31-9	sFlt-1	56048.1	60101.7	245.2
25-2	1x PBS	-3253.7	799.8	28.3
30-5	1x PBS	-4043.6	10.00	3.2
30-6	1x PBS	2227.1	6280.7	79.3

Figure 1 – Minitab output for a 2-sample *t*-test comparing the difference in area between implanted and unimplanted eyes of embryos receiving 100 µg/ml sFlt-1 versus 1x PBS at 1 day post-surgery.

```

Two-Sample T-Test and CI: Sqrt (diff + c), sFlt-1, Sqrt (diff + c), 1x PBS

Two-sample T for Sqrt (diff + c), sFlt-1 vs Sqrt (diff + c), 1x PBS

          N   Mean   StDev   SE
Sqrt (diff + c)  11  147    118    35
Sqrt (diff + c),  3  36.9   38.8   22

Difference = mu (Sqrt (diff + c), sFlt-1) - mu (Sqrt (diff + c), 1x PBS)
Estimate for difference: 110.327
95% CI for difference: (16.924, 203.730)
T-Test of difference = 0 (vs not =): T-Value = 2.63  P-Value = 0.025  DF = 10

```

Figure 2 – Minitab output for a 2-sample *t*-test comparing the difference in area between implanted and unimplanted eyes of embryos receiving 100 µg/ml sFlt-1 versus 1x PBS at 1 day post-surgery with the highest value in the sFlt-1 group removed.

```

Two-Sample T-Test and CI: Sqrt (diff + c), Sqrt (diff + c),

Two-sample T for Sqrt (diff + c), sFlt-1, -out1 vs Sqrt (diff + c), 1x PBS

          N   Mean   StDev   SE
Sqrt (diff + c),  10  116.2  59.9   19
Sqrt (diff + c),  3  36.9   38.8   22

Difference = mu (Sqrt (diff + c), sFlt-1, -out1) - mu (Sqrt (diff + c), 1x PBS)
Estimate for difference: 79.3043
95% CI for difference: (3.9134, 154.6951)
T-Test of difference = 0 (vs not =): T-Value = 2.70  P-Value = 0.043  DF = 5

```

Appendix I – Severity of Ossicle Mispatterning

Table 4 – Classification of embryos according to treatment (sFlt-1 versus 1x PBS), stage of implantation, stage of fixation, treatment time (1-2 days), papilla of implantation, and severity of ossicle mispatterning.

Experiment Number	Treatment	Stage implanted	Stage fixed	Treatment time (days)	Papilla implanted	Mispatterning	
						Implanted eye	Unimplanted eye
13-6	sFlt-1	35	36	1	6	Moderate	Moderate
14-7	sFlt-1	35	36	1	6	Mild	Mild
14-9	sFlt-1	35	36	1	5	Moderate	Normal
25-1	sFlt-1	35.5	36	1	8	Moderate	Mild
25-5	sFlt-1	36	36.5	1	11	Moderate	Moderate
29-5	sFlt-1	34.5	36	1	12	Severe	Normal
30-1	sFlt-1	35.5	36.5	1	7	Mild	Mild
30-4	sFlt-1	35.5	36.5	1	8	Moderate	Mild
31-2	sFlt-1	35	36	1	12	Severe	Moderate
31-8	sFlt-1	35.5	36.5	1	7	Moderate	Normal
31-9	sFlt-1	35.5	36.5	1	7	Mild	Mild

Experiment Number	Treatment	Stage implanted	Stage fixed	Treatment time (days)	Papilla implanted	Mispatterning	
						Implanted eye	Unimplanted eye
12-8	1x PBS	35	36	1	7	Mild	Normal
25-2	1x PBS	35.5	36	1	8	Normal	Normal
30-5	1x PBS	35.5	36.5	1	7	Normal	Normal
30-6	1x PBS	35.5	36.5	1	8	Normal	Normal
16-2	sFlt-1	35	37	2	Antero-dorsal	Mild	Mild
16-3	sFlt-1	35	37	2	Antero-dorsal	Normal	Severe
18-1	sFlt-1	35	37	2	3	Severe	Normal
18-2	sFlt-1	35	36.5	2	Antero-dorsal	Moderate	Moderate
20-1	sFlt-1	35	37	2	7	Severe	Severe
20-2	sFlt-1	35	37	2	3	Severe	Severe
22-1	sFlt-1	35	37	2	10	Normal	Normal
22-2	sFlt-1	35	37	2	5	Mild	Normal

Experiment Number	Treatment	Stage implanted	Stage fixed	Treatment time (days)	Papilla implanted	Mispatterning	
						Implanted eye	Unimplanted eye
22-3	sFlt-1	35	37	2	3	Moderate	Moderate
22-4	sFlt-1	35	37	2	10	Mild	Normal
22-5	sFlt-1	35	37	2	8	Moderate	Normal
22-6	sFlt-1	36	37.5	2	7	Normal	Normal
24-2	sFlt-1	34.5	36	2	12	Severe	Severe
24-3	sFlt-1	34	36	2	14	Moderate	Moderate
24-7	sFlt-1	35	37	2	12	Moderate	Mild
24-9	sFlt-1	35	37	2	12	Normal	Normal
28-1	sFlt-1	35	37	2	12	Mild	Severe
28-3	sFlt-1	35	37	2	12	Mild	Normal
28-4	sFlt-1	35	37	2	12	Normal	Normal
28-5	sFlt-1	34.5	36.5	2	7	Severe	Severe
28-6	sFlt-1	35	37	2	1	Moderate	Severe
28-7	sFlt-1	35	36.5	2	9	Moderate	Moderate

Experiment Number	Treatment	Stage implanted	Stage fixed	Treatment time (days)	Papilla implanted	Mispatterning	
						Implanted eye	Unimplanted eye
26-3	1x PBS	35	37	2	7	Normal	Normal
26-4	1x PBS	35	37	2	7	Normal	Normal
26-5	1x PBS	35	37	2	12	Normal	Normal
26-6	1x PBS	35	37	2	12	Normal	Severe

Discluded from analysis